July 2020

Response of Transient Base Level Signals to Erodibility Contrasts in Bedrock Streams

Joshua A. Wolpert
Louisiana State University and Agricultural and Mechanical College

RESPONSE OF TRANSIENT BASE LEVEL SIGNALS TO ERODIBILITY CONTRASTS IN BEDROCK STREAMS

A Thesis
Submitted to the Graduate Faculty of the
Louisiana State University and
Agricultural and Mechanical College
in partial fulfillment of the
requirements for the degree of
Master of Science

in

The Department of Geology and Geophysics

by
Joshua Alexander Wolpert
B.A., Hamilton College, 2016
August 2020

Acknowledgements

I would like to thank my advisor, Dr. Adam Forte, for his superb guidance and encouragement to pursue this project. I would also like to thank Dr. Karen Luttrell and Dr. Kory Konsoer for their careful thoughts and advice during committee meetings. Lastly, thank you to my peers in the department for richening my LSU experience.

Table of Contents

Abstract

It has long been recognized that bedrock streams gradually adjust their slopes towards topographic steady state, an equilibrium state between rock uplift rate and erosion rate. Tectonic geomorphology studies often analyze stream profiles for clues of this adjustment, which can initiate from changes in tectonic and climatic forcings. The stream power incision model, the most widely utilized framework with which to interpret bedrock stream profiles, predicts that streams perturbed from topographic steady state by changes in bedrock erodibility or uplift rate adjust their slopes to return to topographic steady state through upstream propagating waves of incision, or knickpoints. Under the assumptions of uniform bedrock erodibility and topographic steady state prior to a change in boundary conditions, these knickpoints are predicted to propagate upstream at uniform vertical velocities and celerities set by the stream's erodibility and contributing drainage area. Using a commonly employed 1-D model, this study tests the validity of steady state assumptions of knickpoint behavior when stream profiles are influenced by non-vertical contacts. Deviations in the behavior of knickpoints from steady state assumptions are found to increase as a function of the contact's along-stream celerity and change in erodibility. This results from non-vertical contacts acting as non-stable base levels that alter the uplift rates to which upstream reaches adjust. While this study evaluates highly simplified model scenarios to assess knickpoint elevation, celerity, and prominence as a function of contact dip, change in erodibility, change in uplift rate, and stratigraphy, it demonstrates that steady state assumptions of the stream power incision model break down upstream of non-vertical contacts separating reaches with contrasting rock erodibility.

1. Introduction

Bedrock streams reflect boundary conditions by adjusting their profiles in response to changes in tectonics, climate, and lithology (Kirby and Whipple, 2012; Whittaker, 2012; Wobus et al., 2006). As such, the analysis of bedrock stream morphology has served as an integral component to many tectonic geomorphology studies (Adams et al., 2016; Boulton, 2020; Foster and Kelsey, 2012; Kirby and Whipple, 2012; Mitchell and Yanites, 2019; Rossi et al., 2017; Schoenbohm et al., 2004). Over the past several decades, advances in modeling detachment-limited fluvial incision have established a robust theoretical framework with which to interpret observations (e.g., Howard and Kerby, 1983; Lague et al., 2005; Whipple and Tucker, 1999). Meanwhile, breakthroughs in quantifying erosion rates through catchment-averaged cosmogenic nuclide dating and enhanced availability of high-resolution topography and climate data have helped test geomorphic models and calibrate their parameters (e.g., DiBiase et al., 2010; Ouimet et al., 2009). While consensus on the general behavior of bedrock incision exists, much attention now focuses on more dynamic processes, including stream capture and drainage divide mobility (e.g., Whipple et al., 2017; Willett et al., 2014; Yang et al., 2015), runoff variability and erosion thresholds (e.g., DiBiase and Whipple, 2011; Lague et al., 2005; Rossi et al., 2016), channel width adjustment to changes in uplift rates (e.g., Finnegan et al., 2005), and erosional and morphological response to non-uniform erosional efficiency (Cook et al., 2009; Forte et al., 2016; Giachetta et al., 2014; Mitchell and Yanites, 2019; Perne et al., 2017). This study explores the latter of these processes, and specifically, how variable bedrock erodibility influences transient signals in stream profiles.

Stream profile analysis often utilizes the stream power incision model (SPIM), which, in its simplest state, describes detachment-limited erosion as a function of an erosional efficiency constant (used here interchangeably with erodibility), contributing drainage area, and channel slope (Howard and Kerby, 1983; Whipple and Tucker, 1999). In the SPIM, changes in climate, tectonics, and erodibility initiate upstream propagating kinematic waves of erosion (termed knickpoints or knickzones) that divide profiles into reaches adjusted to different forcings. When a landscape with uniform erodibility experiences a change in uplift rate or rate of base level change, analytical solutions predict for these knickpoints to propagate upstream from the stream's outlet at a vertical velocity set by the landscape's initial and final uplift rates (Niemann et al., 2001). Studies frequently cite this expectation when investigating uplift gradients (Boulton, 2020; Rossi et al., 2017) and drivers of transience in landscapes (Foster and Kelsey, 2012; Lavé and Avouac, 2001; Mitchell and Yanites, 2019) by comparing the elevations of knickpoints on multiple streams.

Analytical solutions supporting a constant knickpoint vertical velocity inherently assume a constant and uniform erodibility (Niemann et al., 2001; Perron and Royden, 2013). However, in natural settings, erodibility is notoriously difficult to measure (Bernard et al., 2019; Roy et al., 2016; Snyder, 2000; Stock and Montgomery, 1999) and is theorized to change with a number of factors that can reasonably vary along a stream's length, including lithology, bedrock jointing, and suspended sediment load (Whipple and Tucker, 1999).

Recently, efforts have addressed understanding the influence of varying rock erodibility on stream profile morphology and erosion rates (Beeson and McCoy, 2020;

Forte et al., 2016; Perne et al., 2017; Yanites et al., 2017). Forte et al. (2016) conducted 2-D landscape evolution modeling experiments and demonstrated that topographic steady state (a state where erosion rates match uplift rates at all locations in a profile) is unlikely to exist in landscapes with multiple rock units with non-vertical contact dips, and complex patterns of stream steepness and erosion rates can result from spatially variable erodibility. This study found the complexity of stream profile morphology and erosion rates to largely depend upon stratigraphic order and contact dip, with near-horizontal contacts producing profiles deviating most from topographic steady state. Using an analytical approach, Perne et al. (2017) argued that the morphology of streams with layered stratigraphy reflects a competition between topographic steady state and erosional continuity, which posits that locations upstream and downstream of a contact share identical erosion rates in the long term. This condition not only explains behavior described by Forte et al. (2016), where profiles deviate in form from those predicted by topographic steady state, but also predicts the creation of an upstream-propagating wave of incision accompanying a new lithology's exposure at a stream's outlet. These studies converge towards a conclusion that layered stratigraphy complicates stream profile analysis because, at any given location, steepness reflects base level history, downstream adjustment to changes in erodibility (a function of dip angle and change in erosional efficiency), and local erosional efficiency (Forte et al., 2016; Perne et al., 2017; Yanites et al., 2017). In their modeling work investigating topography with layered stratigraphy and varying uplift rates, Yanites et al. (2017) aptly described the difficulty of interpreting landscapes where transient signals of layered stratigraphy coexist with transient signals of

base level change. They also observe that uplift-induced waves of erosion tend to diffuse after interacting with contacts.

Due to: 1) the prevalence of studies utilizing knickpoint distributions throughout landscapes, 2) the documented difficulty in measuring erosional efficiency, and 3) the complex behavior of landscapes with non-vertical spatial variability in erosional efficiency (e.g., non-vertical rock contacts), I explore the influence of layered stratigraphy on transient uplift-induced knickpoints in bedrock stream profiles. I solve the SPIM with a commonly used 1-D finite difference scheme (Campforts and Govers, 2015; Czarnota et al., 2014) to test parameter space for influences on stream morphology, knickpoint vertical velocity and celerity, and knickpoint prominence along a profile. The parameters tested include contact dip angle, cross-contact change in erodibility (referred to here as the K_f/K_i ratio), the magnitude of uplift rate change, and the thickness and order of layered stratigraphic units. These analyses reveal that steady state assumptions fail to hold when non-vertical contacts exist in streams because, as noted by Forte et al. (2016) and Perne et al. (2017), non-vertical contacts perturb upstream reaches. I then demonstrate that the celerity of a contact along a stream profile and cross-contact change in erodibility influence the degree to which upstream reaches deviate from steady state. Using steady state assumptions of knickpoint vertical velocity and celerity, I isolate the effect of this perturbation to altering the initial uplift rate of reaches upstream of contacts. Lastly, I explore scenarios with more than two units and find that deviations between an uplift knickpoint's behavior in a stream with non-vertical rock contacts and its predicted behavior in a steady state stream result from the knickpoint's and each rock unit's interactions with secondary incisional waves produced by contacts. While profiles with

steep contacts differ only slightly from those with spatially uniform erodibility, shallowly dipping contacts cause greater deviations from steady state assumptions, potentially complicating interpretations of uplift driven knickpoints in natural settings.

2. Background

2.1. Overview of the Stream Power Incision Model

The stream power incision model (SPIM) assumes a power law relationship between detachment-limited incision rate (ε) and stream power (bed shear stress times mean water velocity). A common and simple derivation of the SPIM, ignoring thresholds for erosion, involves estimating mean bed shear stress by discharge, bankfull width, and local slope, such that ε is expressed in terms of catchment and stream bed properties:

$$\varepsilon = KA^m S^n \quad (1)$$

where A is drainage area (L^2) and used as a proxy for discharge, S is local channel slope, and m and n are positive constants known as the area and slope exponents, respectively. In this version of the SPIM, m reflects erosion process, basin hydrology, and hydraulic geometry, whereas n is solely a function of erosion process. In equation (1), K is an erosional efficiency constant (LT^{-1}), which lumps together several parameters related to channel width, climate, and erosion thresholds (Kirby and Whipple, 2012; Stock and Montgomery, 1999; Whipple and Tucker, 1999).

Equation (1) is commonly written in mass-balance form with rock uplift or base level fall to describe the evolution of a stream profile as a non-linear kinematic wave equation (Howard, 1994; Whipple and Tucker, 1999):

$$\frac{\partial z}{\partial t} = U(x,t) - K(x,t)A(x,t)^m \left|\frac{\partial z}{\partial x}\right|^n \quad (2)$$

where $\frac{\partial z}{\partial x}$ is the local slope (L) and $U(x,t)$ is the rate of rock uplift or base level fall. Equation (2) captures the long-observed tendency for streams to reach a 'graded' state, or equilibrate their morphologies to approach topographic steady state (Howard, 1994; Kirby

and Whipple, 2012; Wobus et al., 2006). Under the assumption of topographic steady state, equation (2) can be integrated with respect to contributing drainage area from a stream's outlet (x_b) to an along-stream position (x) to solve for elevation (z):

$$z(x) = z(x_b) + \left(\frac{U}{K{A_o}^m}\right)^{1/n}\chi \quad (3)$$

$$\chi = \int_{x_b}^{x}\left(\frac{A_0}{A(x)}\right)^{\frac{m}{n}} dx \quad (4)$$

where A_o is a reference drainage area, and χ emerges as a transformation of along-stream distance (Royden and Taylor Perron, 2013). Alternatively, equation (2) at steady state can be solved for slope, such that:

$$S = \left(\frac{U}{K}\right)^{1/n} A^{-m/n} \quad (5)$$

When A (at a given x), m, and n are held fixed, equation (5) highlights the dependency of a stream's slope on the ratio of uplift rate to erodibility, as predicted by the SPIM. Conveniently, when viewing stream profiles in χ-transformed space with A_o set to unity, this ratio raised to the $1/n$ power is the slope of the transformed profile (Fig. 1).

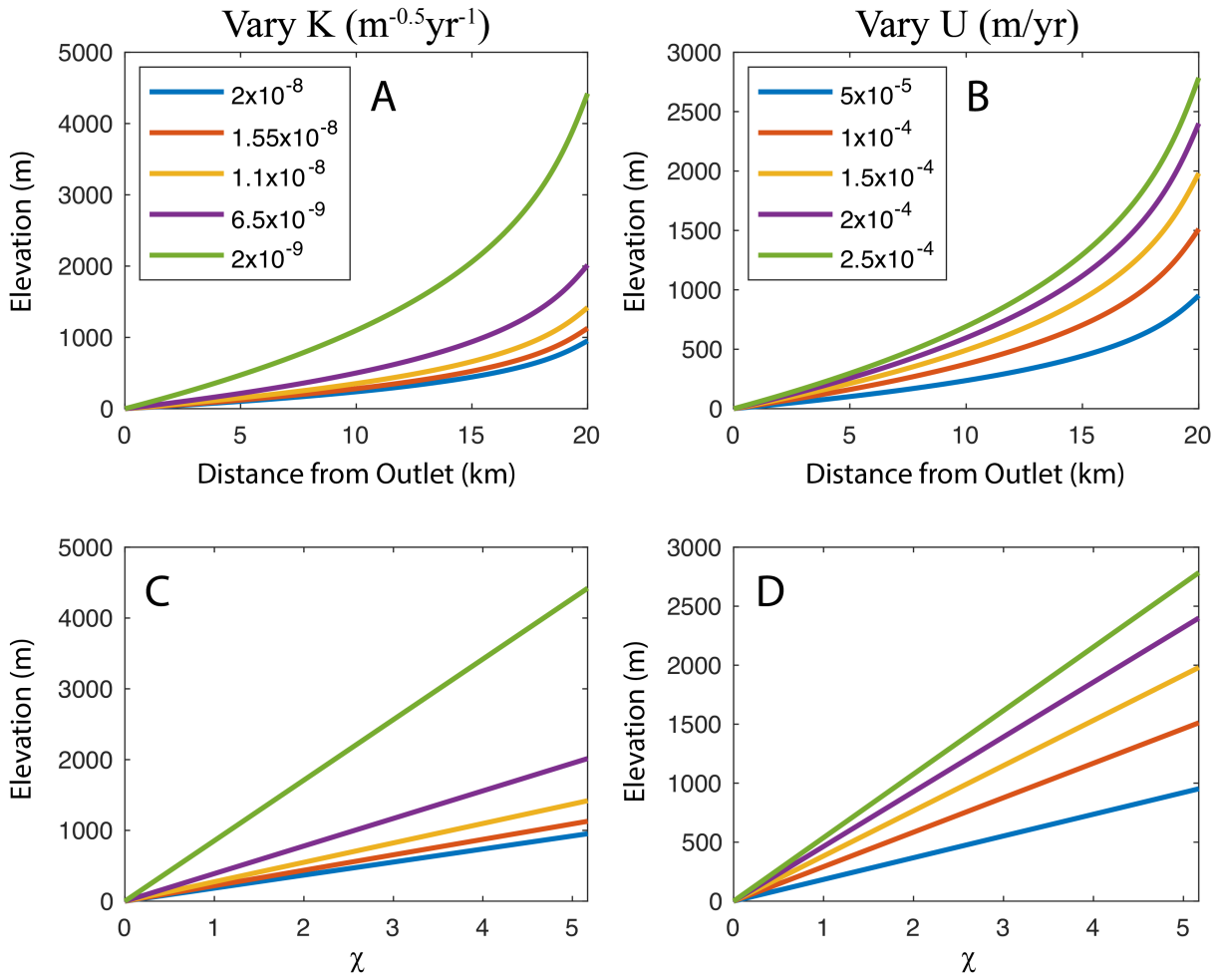

Fig 1. Steady-state stream profiles in normal (A and B) and χ-space (C and D) with varying erodibilities (A and C) and uplift rates (B and D). The uplift rate for profiles in panels A and C is 5×10^{-5} m/yr, and the erodibility for profiles in panels B and D is 2×10^{-8} $m^{-0.5}yr^{-1}$. n is 1.5 and m is 0.75 for all profiles.

2.2. Interpreting Tectonics and Climate from Stream Profiles

Independent from the SPIM, Flint's Law describes the natural concavity of stream profiles (i.e., decreasing slope with increasing drainage area), such that:

$$S = k_s A^{-\theta} \quad (6)$$

where k_s and θ are known as the channel steepness and concavity index, respectively (Flint, 1974; Hack, 1957). Both of these metrics can be solved for on log-log plots of slope vs. area (slope-area plots), where k_s is the y-intercept and θ is the slope of a linear regression. Since

equation (6) indicates covariance between k_s and θ, k_s is often calculated using a fixed reference concavity, θ_{ref}, enabling meaningful comparison between different streams:

$$S = k_{sn}A^{-\theta_{ref}} \quad (7)$$

where k_{sn} is known as the normalized channel steepness index and has been shown to positively correlate with other metrics of topographic steepness such as mean relief and mean hillslope gradient (Wobus et al., 2006). When Flint's Law is put into the context of the SPIM:

$$k_{sn} = \left(\frac{U}{K}\right)^{1/n} \quad (8)$$

It is worth emphasizing that θ_{ref}, which equates to the ratio of m/n in the context of the SPIM, has been found to be insensitive to uplift rate across a given setting (Kirby and Whipple, 2012) and typically ranges between 0.35-0.60 (Wobus et al., 2006). In contrast, k_{sn} has been found to correlate with uplift rate, as evidenced by cosmogenic erosion rates (Cyr et al., 2010; DiBiase et al., 2010; Ouimet et al., 2009). Equation (8) is identical to the coefficient for χ in equation (3) when A_0 is set to unity, which means k_{sn} can also be calculated as the slope of χ-transformed stream profiles (Perron and Royden, 2013).

2.3. Stream Profile Responses to Perturbations from Steady State

As predicted by equation (5), if drainage area and concavity are held fixed, the slopes (and thus elevations) of stream profiles will adjust to changes in uplift rate (U) or erodibility (K). This adjustment occurs progressively through an upstream migrating wave of incision, which propagates throughout the drainage network (Whipple and Tucker, 1999). These transient slope-break knickpoints (herein referred to as uplift knickpoints) can be identified as a change in the scaling between slope and drainage area (i.e., k_{sn}) and represent the boundary between relict upstream reaches that erode at a rate set by a

previous U and/or K and downstream reaches that have adjusted to new boundary conditions (Howard, 1994; Kirby and Whipple, 2012; Wobus et al., 2006).

Assuming constant erodibility along a stream's length, the vertical velocity of uplift knickpoints is predicted to be independent of erodibility (Niemann et al., 2001), such that:

$$V_v = \begin{cases} (U_2 - U_1)\left(\dfrac{\left(\frac{U_2}{K}\right)^{1/n}}{\left(\frac{U_2}{K}\right)^{1/n} - \left(\frac{U_1}{K}\right)^{1/n}}\right) & for\ n > 1 \quad (10a) \\ U_2 & for\ n = 1 \quad (10b) \\ U_2 + (n-1)U_1 & for\ n < 1 \quad (10c) \end{cases}$$

where V_v is the predicted knickpoint vertical velocity (Mitchell and Yanites, 2019; Perron and Royden, 2013). V_v is sensitive to the value of n, and this study focuses mostly on the case of $n > 1$, which is likely the most commonly encountered condition in natural settings (DiBiase and Whipple, 2011; Harel et al., 2016; Lague, 2014; Ouimet et al., 2009). However, regardless of the value of n, V_v will not vary with K, so long as K remains constant along a stream's length (i.e., K in equation (10) cancels out if n is independent of K). Therefore, given the common assumption of n's invariability within a rock type (Whipple et al., 2000), knickpoint elevations at any given time simply reflect the initial and/or new uplift rate, depending on the value of n (Mitchell and Yanites, 2019). Since under the previously-described conditions, an incisional wave caused by a change in uplift rate propagates at a uniform and constant vertical velocity through concave streams, the incisional wave's celerity (C) scales with upstream drainage area (Whipple and Tucker, 1999), such that:

$$C = KA^m S^{n-1} \quad (11)$$

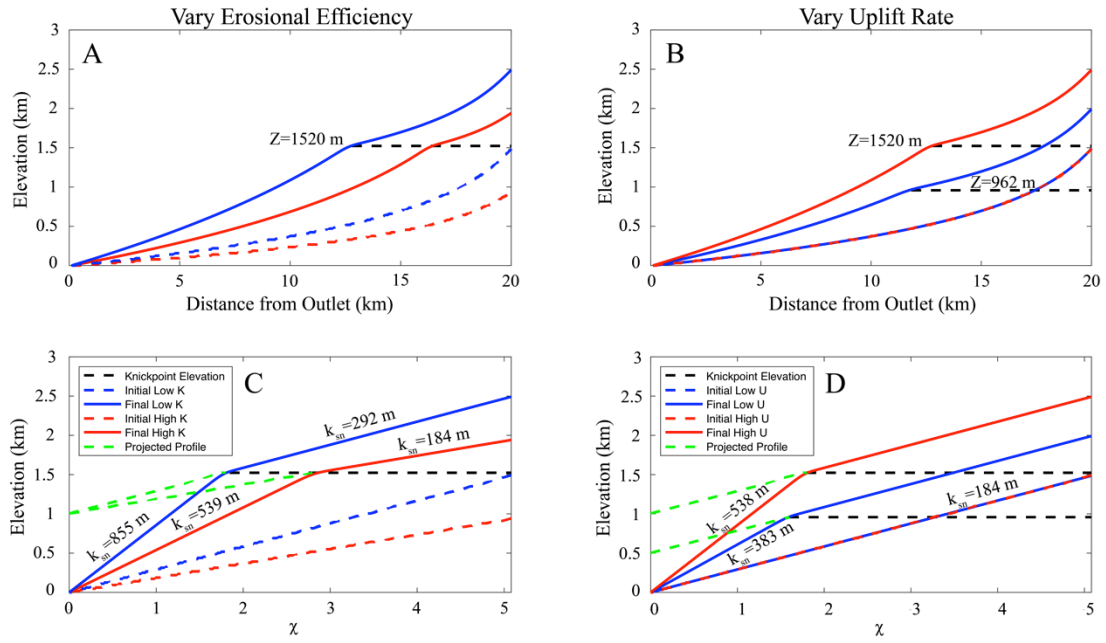

Fig 2. Example stream profiles in normal (A and B) and χ-space (C and D) 5 Myr after a step change in uplift rate and n=1.5. The initial uplift rates for all profiles is 5×10^{-5} m/yr. Panels A and C show profiles with constant but different erodibilities (2×10^{-8} $m^{-0.5}yr^{-1}$ and 1×10^{-8} $m^{-0.5}yr^{-1}$) and identical final uplift rates (2.5×10^{-4} m/yr). Panels B and D show profiles with constant and identical erodibilities ($1\times10^{-8}m^{-0.5}yr^{-1}$) but different final uplift rates (1.5×10^{-4} m/yr and 2.5×10^{-4} m/yr). Green dashed lines show projections of reaches upstream from knickpoints to stream outlets.

In χ-space, this horizontal celerity (V_χ) is constant (Mitchell and Yanites, 2019; Royden and Taylor Perron, 2013), such that:

$$V_\chi = \begin{cases} \dfrac{U_2 - U_1}{\left(\left(\frac{U_2}{K}\right)^{1/n} - \left(\frac{U_1}{K}\right)^{1/n}\right) A_0^{\,-m/n}} & for\ n > 1 \quad (12a) \\ K A_0^{\,m/n} & for\ n = 1 \quad (12b) \\ \dfrac{n U_1}{\left(\frac{U_1}{K}\right)^{1/n} A_0^{\,-m/n}} & for\ n < 1 \quad (12c) \end{cases}$$

A stream profile's response to the exposure of contrasts in erodibility (i.e., rock contacts) at its outlet can be explained conceptually by the competition between topographic steady state and erosional continuity; that is, the condition that rocks on either side of a contact equilibrate towards a state where erosion rates in the direction of the

contact dip are equal (Perne et al., 2017). If this condition is violated, overhanging or protruding reaches develop up or downstream from the contact. As these protrusions enlarge, they are eventually undercut and/or eroded, thereby driving the stream towards erosional continuity in the long run.

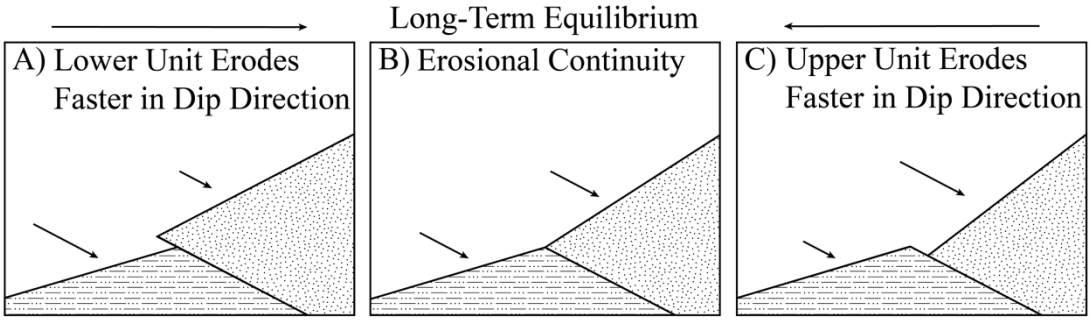

Fig 3. Overview of erosional continuity with negative contact dips. If the upper unit erodes slower than the lower unit (A), erosion rates at the protruding reach will increase to approach a long-term equilibrium state of erosional continuity (B). Likewise, if the lower unit erodes slower than the upper unit (C), erosion rates downstream from the contact will increase to drive the system towards erosional continuity. Figure modified from Perne et al. (2017).

Topographic steady state maintains erosional continuity when contacts are vertical, since the direction parallel to the contact is the vertical uplift component. However, as contact dips shallow, erosional continuity requires erosion rates that deviate further from topographic steady state. Perne et al. (2017) suggest that the rapid erosion of protruding segments near contacts provides physical reasoning to the existence of perturbations driven by erodibility contrasts in their modeling work. For the case of horizontal contacts, these perturbations (herein referred to as transient contact knickpoints) migrate upstream with celerity (C_{tc}) in χ-space:

$$C_{tc} = U^{(n-1)/n} K^{1/n} A_0^{m/n} \quad (11)$$

Thus, a stream profile's response to the exposure of a contact between rocks with different erodibilities at its outlet is two-fold (Fig. 4): 1) a knickpoint caused by a change in

erodibility remains at or near the contact (Forte et al., 2016; Kirby and Whipple, 2012), and 2) a transient, often subtler, knickpoint propagates upstream as a result of the profile's adjustment to maintain erosional continuity (Perne et al., 2017; Yanites et al., 2017).

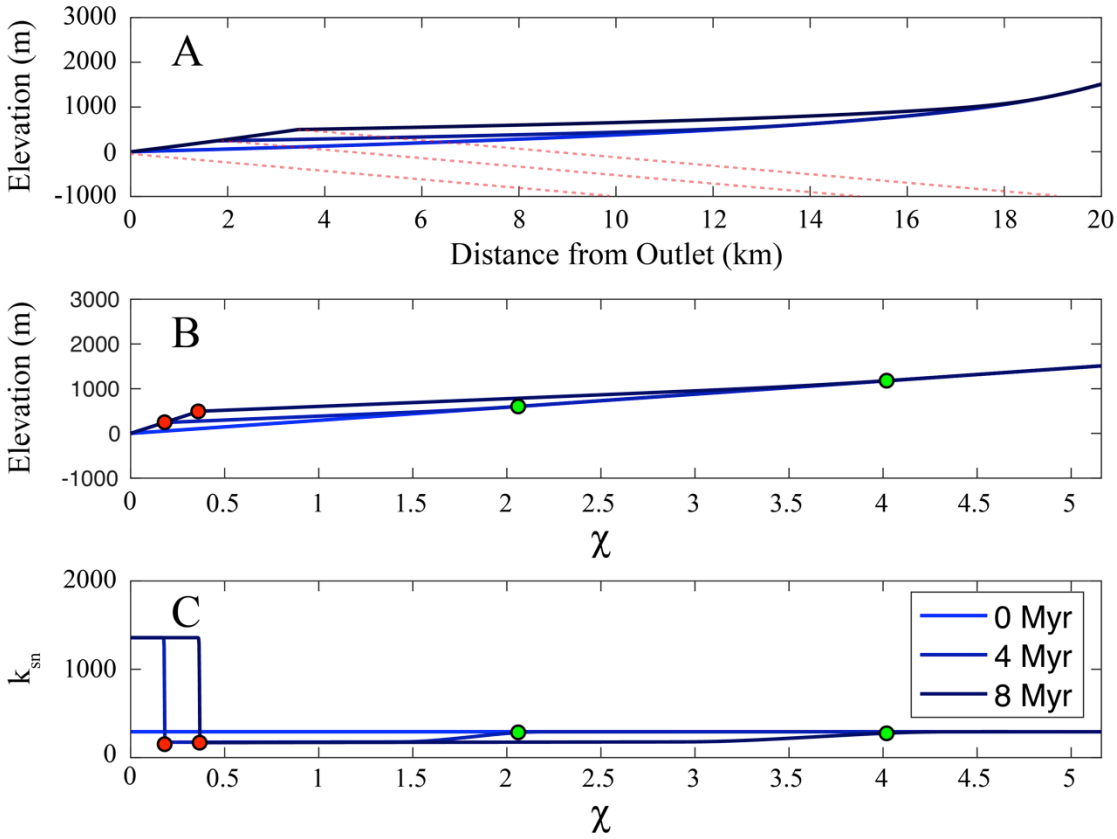

Fig 4. Time slices of a stream profile after exhumation of a new lithology at the stream's outlet in real space (A), χ-space (B), and $\chi - k_{sn}$ space (C). Uplift rate is constant at $1x10^{-4}$ m/yr. The upper unit's K is $2x10^{-8}$ $m^{-0.5}yr^{-1}$, the lower unit's K is $2x10^{-9}$ $m^{-0.5}yr^{-1}$, and the contact dip is 5 degrees towards the basin divide. Note the dual-component response with one knickpoint locked near the contact (red dot) and a second subtle transient contact knickpoint propagating upstream ahead of the contact (green dot). In panel (A), the dashed red lines show the contact at each time step. The contact is not yet exhumed at the stream's outlet at time 0.

3. Methods

3.1. Model Description

I built a 1-D stream profile model to explore the influence of varying lithology on stream profiles adjusting to changes in uplift rate (Fig. 5). The model solves equation (2) numerically with an explicit upwind differencing scheme (Campforts and Govers, 2015):

$$z_i^{k+1} - z_i^k = \left[U - KA_i^m \left(-\frac{z_{i+1}^k - z_i^k}{\Delta x}\right)^n\right]\Delta t \qquad (12)$$

where i is node position along a profile, and k is time step. At each time step, the model evaluates the profile for numerical stability with a Neumann stability analysis using the Courant-Friedrichs-Lewy (CFL) criterion (Campforts and Govers, 2015).

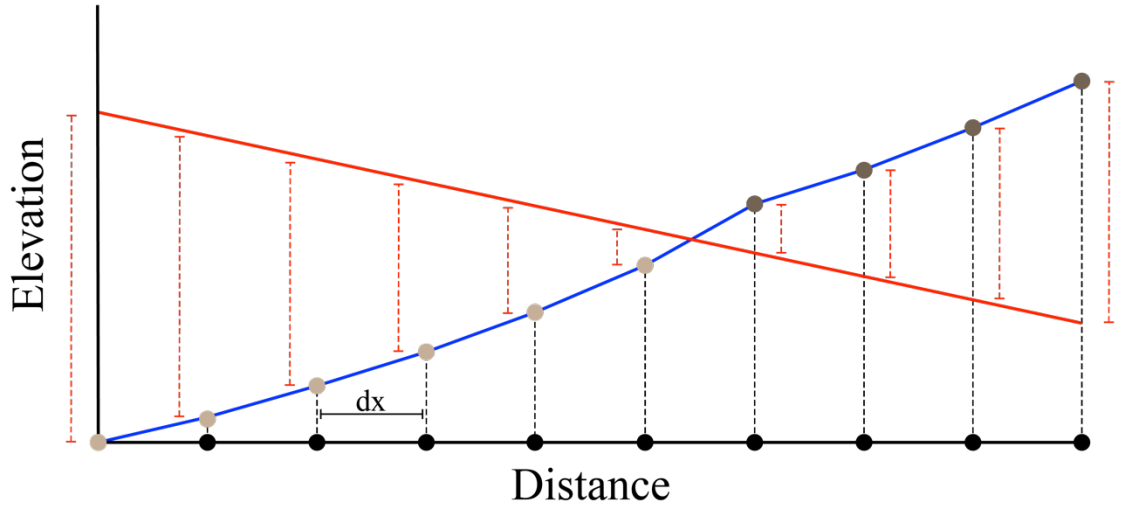

Fig. 5. Overview of model domain. The light and dark brown dots are nodes (colored by K), the blue line is the stream profile, the red continuous line is a contact, black dashed lines are elevations at each node, and red dashed lines are elevation differences between the stream profile and contact at each node. The model records the information represented by the dashed lines at each node during each time step to evolve the profile and determine which unit is exposed.

I fixed the model's downstream boundary at zero and established initial conditions using equations (3) and (4). I used Hack's Law (Hack, 1957) to determine the relationship between downstream distance from the divide and contributing drainage area:

$$A = A_i + cx^h \quad (13)$$

where A_i is a critical drainage area marking the transition from colluvial to alluvial conditions, and c and h are positive values commonly referred to as the Hack coefficient and Hack exponent, respectively.

The model treats planar contacts as abrupt spatial changes in K, and each contact is stored as elevation values that are updated at each node during each time step. Changes in uplift rate occur instantaneously and are applied uniformly to a stream's entire length, thereby simulating block uplift or base level fall. The model operates as a stand-alone function that allows full user control over SPIM and Hack's Law parameters (See Section 7).

3.2. Modeled Scenarios

The slope exponent, n, can be estimated as the exponent of a fit between a population of catchment-averaged erosion rates and catchment-averaged channel steepness and is most often calculated as greater than 1 (DiBiase and Whipple, 2011; Harel et al., 2016; Lague, 2014; Ouimet et al., 2009) but has been found to range between ~2/3 and ~5/3 (e.g., Larimer et al., 2019; Whipple et al., 2000). Therefore, I focused on cases in which the slope exponent is 3/2, but following in similar studies' footsteps (e.g., Beeson and McCoy, 2020; Perne et al., 2017), I ran complimentary simulations in which n is equal to 2/3 and 1 to check the sensitivity of my findings to the slope exponent.

I ran an initial 360 baseline runs to test parameter space by varying the ratio of K upstream and downstream of a contact (also referred to as the K_f/K_i ratio) and the dip angle of contacts (Table 1). I varied the K_f/K_i ratio greater than an order of magnitude for each dip angle tested, and K values are based on previous modeling studies (e.g., Mitchell and Yanites, 2019; Whipple and Tucker, 1999). Results are presented for

horizontal, 5°, 15°, 30°, and 45° dips, with non-horizontal dips tested in both the positive (toward the outlet) and negative (toward the divide) directions. I also performed preliminary test runs with dips exceeding 45°, but under these conditions, the uplift knickpoint's behavior closely matched steady state predictions. All runs began with U_1 set to $5x10^{-5}$ m/yr, and the propagation of uplift knickpoints were initiated through both small (U_2=$1x10^{-4}$ m/yr, ΔU=$5x10^{-5}$ m/yr) and large (U_2=$2.5x10^{-4}$ m/yr, ΔU=$2x10^{-4}$ m/yr) step changes in U to test the influence of the magnitude of ΔU on outcomes. I used a model domain of a 20 km long profile with nodes spaced 10 m apart (dx). Runs were initially performed with time step intervals (dt) equal to 100 years, and I reduced dt when runs failed the Neumann stability analysis. For all runs, c was set to 6.69 and h was set to 1.67, which are values used in previously published work (Hack, 1957; Perne et al., 2017; Whipple and Tucker, 1999). A_i was set to 1 km^2, a conservative critical drainage area for the transition from diffusive hillslope processes to stream channel incision (Montgomery and Foufoula-Georgiou, 1993). All model runs began with a single erodibility and contacts at depth, and contacts were progressively exposed with an uplift rate set by U_1. After exploring the general behavior of a knickpoint passing through a single contact, I explored more complex scenarios in which profiles contain multiple contacts and uplift knickpoints interact with secondary incisional waves produced by contacts. Parameters for these additional runs are addressed when the runs are discussed.

Table 1. Range of Parameter Values used in Single Contact Baseline Runs.

Stratigraphy	Contact Dip (°)	K_i ($m^{-0.5}yr^{-1}$)	K_f ($m^{-0.5}yr^{-1}$)	U_1 m/yr	U_2 m/yr	n	m
Hard Over Soft	0,-5,-15,-30,-45	$3.8x10^{-8}$	$2x10^{-9}$ - $3.44x10^{-8}$	$5x10^{-5}$	$1x10^{-4}$,$2.5x10^{-4}$	1.5	0.75
Soft Over Hard	0,-5,-15,-30,-45	$2x10^{-9}$	$5.6x10^{-9}$ - $3.8x10^{-8}$	$5x10^{-5}$	$1x10^{-4}$,$2.5x10^{-4}$	1.5	0.75
Hard Over Soft	5,15,30,45	$3.8x10^{-8}$	$1.064x10^{-7}$ - $7.22x10^{-7}$	$5x10^{-5}$	$1x10^{-4}$,$2.5x10^{-4}$	1.5	0.75
Soft Over Hard	5,15,30,45	$3.8x10^{-8}$	$2x10^{-9}$ - $3.44x10^{-8}$	$5x10^{-5}$	$1x10^{-4}$,$2.5x10^{-4}$	1.5	0.75

3.3. Measuring Stream Morphology Metrics

3.3.1. Knickpoint Vertical Velocity

As the model induces knickpoints through temporal changes in U and spatial and temporal changes in K, knickpoints can be detected as abrupt changes (i.e., break points) in mean k_{sn} along a stream profile. These break points are particularly easy to identify on $\chi - k_{sn}$ plots (Fig 4). To avoid bias introduced by manually locating break points from visual inspection of $\chi - k_{sn}$ plots, I automated this process using the 'ischange' MATLAB function.

After identifying knickpoints with arrays of k_{sn} data, I produced knickpoint elevation time series (e.g., Fig. 6) and extracted vertical velocities by isolating data points representing the same knickpoint and calculating the slope of this data via linear regression. When applied to simulations with no contact and a known analytical solution expressed by equations (10a-b), this method reproduces the known vertical velocity to within 0.25% error for a case where $n > 1$ and 1.6% error for a case where $n = 1$. These slight inaccuracies likely result from numerical diffusion associated with the explicit upwind differencing scheme (Campforts and Govers, 2015).

I streamlined the data extraction process with a companion function to the model that allows users to extract data for knickpoints nearest to a line drawn on knickpoint time series. The function records the nearest data point to the drawn line at each time step, allowing users to account for scenarios where multiple knickpoints are detected in the vicinity of a single incisional wave (e.g., the upstream and downstream boundaries of broad knickzones). If multiple knickpoints exist near a single transient wave, users can target the same knickpoint through time by drawing a data extraction line either consistently above

or below a knickpoint elevation path. For scenarios with hard over soft positively dipping contacts, knickpoints were too subtle in the soft unit to be detected by this semi-automated process, and I manually calculated their vertical velocities by recording the knickpoints' elevations at multiple timesteps.

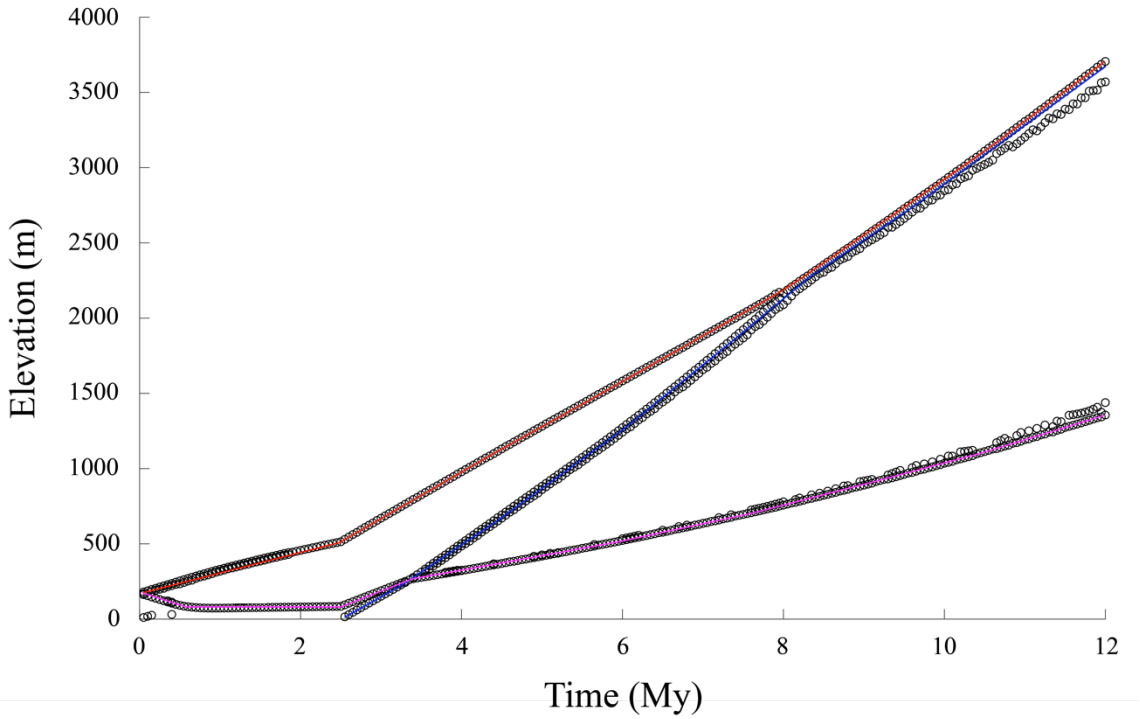

Fig. 6. Example knickpoint time series used to calculate vertical velocities. The run equilibrates for 2.5 My, during which time stable contact (magenta line) and transient contact (red line) knickpoints partition. At 2.5 My the uplift rate changes from 5×10^{-5} m/yr to 2.5×10^{-4} m/yr, and an uplift knickpoint emerges (blue line).

3.3.2. Knickpoint Prominence

I define knickpoint prominence as the absolute value of the change in k_{sn} between reaches upstream and downstream of a knickpoint (also referred to here as the cross-knickpoint change in k_{sn}). The larger a knickpoint's prominence, the more noticeable it is in profile view and χ-space. I arbitrarily chose the Greek letter ψ to represent the cross-knickpoint change in k_{sn}, such that the analytical expectation of ψ is:

$$\psi = \left(\frac{U_{US}}{K_{US}}\right)^{1/n} - \left(\frac{U_{DS}}{K_{DS}}\right)^{1/n} \quad (14)$$

Where the subscripts US and DS indicate the upstream and downstream reaches from a knickpoint, respectively. A positive ψ indicates a concave knickpoint or knickzone, while a negative ψ indicates a convex knickpoint or knickzone. To say a knickpoint has decreased in prominence simply indicates that ψ is closer to zero and does not specify whether the knickpoint is concave or convex.

To measure ψ, I selected single data points on $\chi - k_{sn}$ plots upstream and downstream from knickpoints. I avoided measuring k_{sn} in broad knickzones to avoid influence from numerical diffusion. This method yielded more accurate results than subtracting average k_{sn} values over a constant node distance from knickpoints, and it is appropriate because the model's output lacks noise. In natural settings, where sub-optimal data resolution and imperfect flow routing algorithms commonly produce topographic noise, a more accurate measurement of ψ may result from averaging k_{sn} across a constant length spaced some distance upstream and downstream from a knickpoint.

4. Results

The following sections concern the baseline runs (Table 1) and focus solely on the influence of a single contact on a stream's morphology and uplift knickpoint's behavior. For readability, I refer to results from my model as 'observed' values and steady state predictions as 'predicted' values. Observations from the baseline runs later provide empirical evidence within a broader discussion of how and why knickpoints change upstream from a non-vertical contact (Section 5). As such, the following descriptions of baseline runs include pertinent findings and omit extraneous details. Trends emerging from the baseline runs often suggest nonlinear relations between knickpoint vertical velocity and the tested parameters, and power law and exponential fits were compared using root-mean-square errors to better characterize these trends. As power law fits typically yielded lower (and small) root-mean-square errors, their parameters accompany relevant figures in the following sections. However, a full table of power law and exponential fit parameters for all tested relations is available online (See Section 7). For the remainder of the study, the previously established terminology continues to be used when referencing stream profile features (Fig. 7).

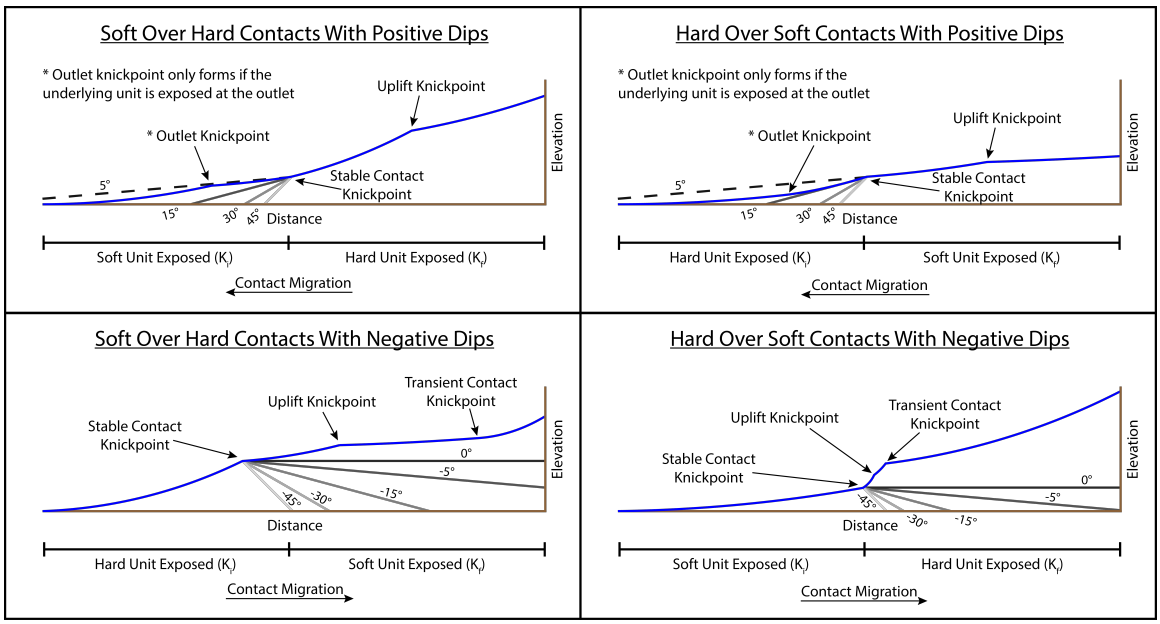

Fig. 7. Simplified diagrams of profiles showing the general behavior of baseline runs. Each panel is annotated with terminology used throughout this study. Note that while commonly discussed features are accentuated, their morphologies vary by parameter values explored in this study.

4.1. Soft Over Hard Contacts with Positive Dips

For runs with soft over hard stratigraphy and contacts with positive dip angles, the contact is first exposed in either the middle (when dips are sufficiently shallow) or head (when dips are sufficiently steep) of the stream. As the contact propagates towards the stream's outlet, newly exposed hard unit reaches upstream of the contact increase k_{sn} but remain under-steepened with respect to the predicted steady state k_{sn} (Fig. 8). As the hard underlying unit's erodibility decreases (i.e., the K_f/K_i ratio approaches 0), the reach upstream of the contact becomes progressively more under-steepened. Additionally, despite the uniform erodibility upstream of the contact, k_{sn} decreases when advancing from the contact to the channel head, and the rate of decrease in k_{sn} scales with the change in K between the soft downstream and hard upstream unit (Fig. 8). This progressive upstream decline in steepness forms a broad convex zone between the contact and the

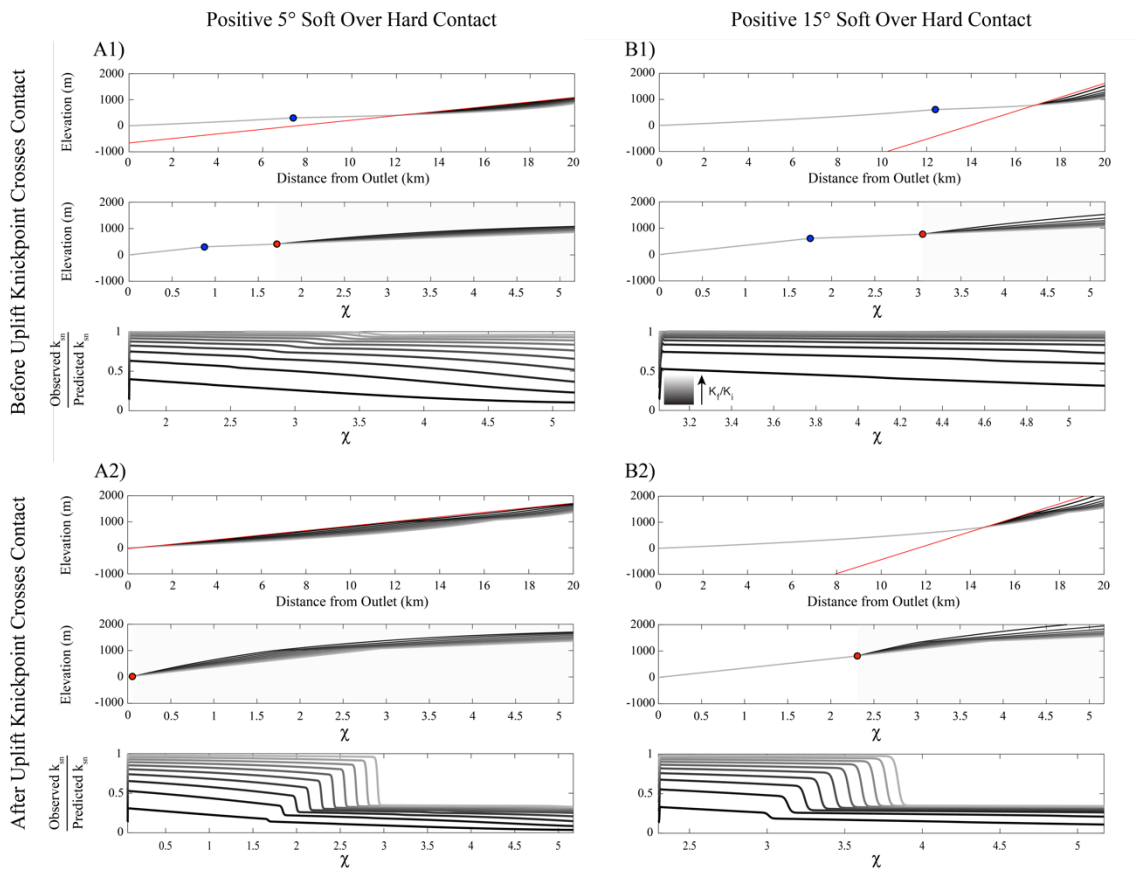

Fig. 8. Runs with soft over hard 5° (A1 and A2) and 15° (B1 and B2) dips and K_f/K_i ratios ranging from 0.05 to 0.91 before (A1 and B1) and after (A2 and B2) an uplift knickpoint crosses a contact. A1 and B1 are 1 Myr and 2 Myr, respectively, after a change in uplift rate from 5x10^{-5} m/yr to 2.5x10^{-4} m/yr. A2 is 3.5 Myr and B2 is 4.5 Myr after the change in uplift rate, respectively. The red lines in panels (A) and (D) are the contacts in regular space, the red dots are the contacts in χ-space, and the blue dots are the uplift knickpoint. The shaded regions in χ-space are the lateral extent of the underlying plots of the ratio of observed to predicted k_{sn}.

channel head in χ-space, a characteristic feature found throughout all of the soft over hard runs with positive contact dips.

Upon propagating into the hard unit, the uplift knickpoint's vertical velocity decreases as a function of both 1) the K_f/K_i ratio, such that propagation into a harder hard

unit (lower K_f) results in a lower knickpoint vertical velocity than propagation into a softer hard unit (higher K_f), and 2) the contact's dip, such that knickpoint vertical velocity

Large Change in Uplift Rate

V_f/V_i Power Law Fits

Dip	Coeff.	Exp.	RMSE
5	3.02×10^{-4}	5.22×10^{-2}	2.82×10^{-6}
15	3.05×10^{-4}	4.71×10^{-2}	1.03×10^{-6}
30	3.08×10^{-4}	4.38×10^{-2}	5.54×10^{-7}
45	3.09×10^{-4}	3.62×10^{-2}	1.04×10^{-6}

Small Change in Uplift Rate

V_f/V_i Power Law Fits

Dip	Coeff.	Exp.	RMSE
5	1.38×10^{-4}	8.82×10^{-2}	5.26×10^{-7}
15	1.40×10^{-4}	6.62×10^{-2}	6.62×10^{-7}
30	1.41×10^{-4}	5.62×10^{-2}	1.05×10^{-6}
45	1.40×10^{-4}	3.76×10^{-2}	1.07×10^{-6}

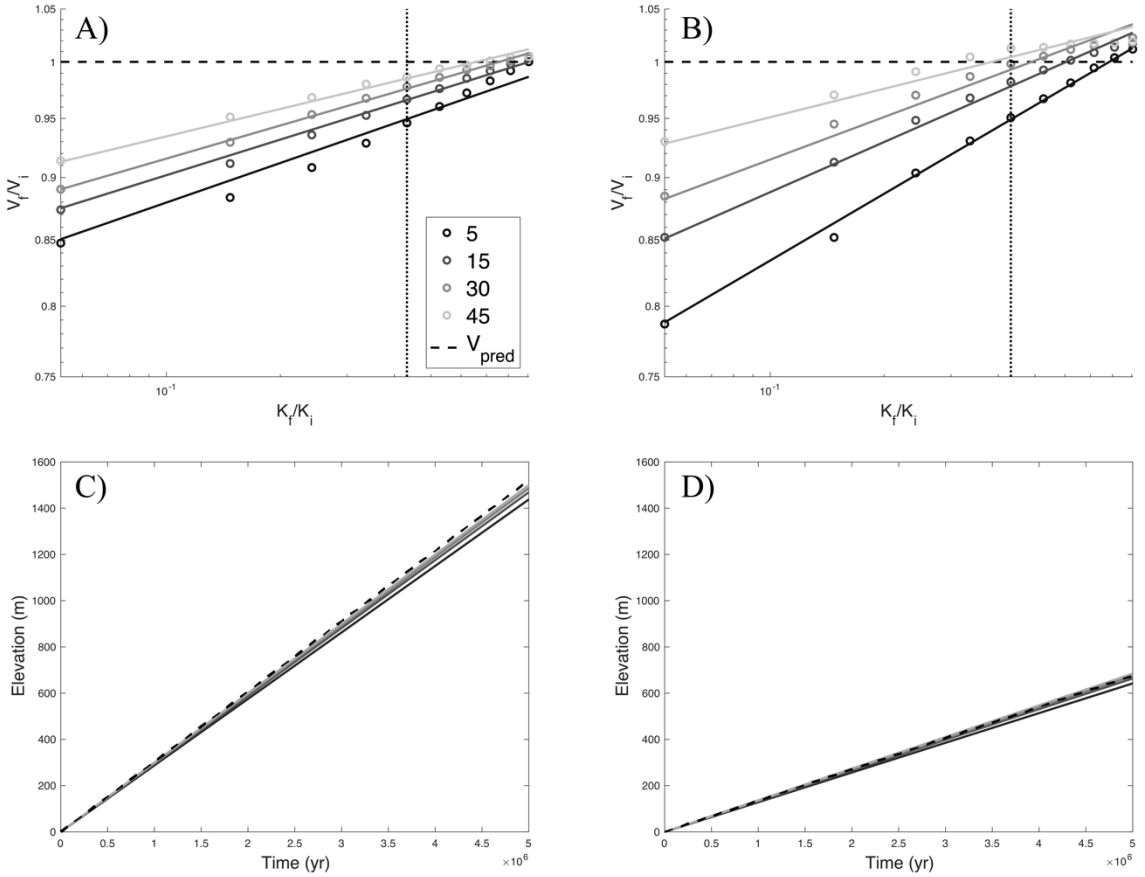

Fig. 9. Influence of the K_f/K_i ratio and contact dip on the vertical velocity of uplift knickpoints after passing soft over hard contacts with positive dips (panels A and B). Panels C and D show time series of uplift knickpoint elevations after passing contacts with varying dips and K_f/K_i ratios equal to 0.122 (dashed vertical lines in panels A and B). In panels C and D, time 0 occurs immediately after uplift knickpoints pass a contact, and elevations are measured with respect to the knickpoint's elevation at time 0.

decreases as that contact's dip shallows. Additionally, the relationships between the K_f/K_i ratio, contact dip angle, and knickpoint vertical velocity are well explained by power laws,

with changes in the model's parameter values primarily causing changes in the power law exponent (Fig. 9). The reach upstream from the contact and downstream from the uplift knickpoint remains under-steepened by a degree that scales inversely with the erodibility of the hard unit. This reach also decreases k_{sn} fom the contact to uplift knickpoint at a rate that increases as dips approach horizontal and the hard unit's K decreases.

The uplift knickpoint's prominence in the hard unit remains fairly constant (increasing by a few units per Myr), is consistently less than the predicted value, and correlates with contact dip angle. Additionally, a complex relationship between the K_f/K_i ratio and the uplift knickpoint's prominence in the hard unit emerges, with prominence increasing as the K_f/K_i ratio decreases up until an inflection point. The location of this inflection point, in terms of the K_f/K_i ratio, depends upon the contact dip angle and the uplift rate responsible for the base level perturbation. When K_f/K_i ratios fail to exceed the inflection point, uplift knickpoint prominence decreases with lower K_f/K_i ratios, and uplift knickpoints prminence can even decrease prominence after entering the hard unit (Fig. 10).

Lastly, the reach upstream from the contact remains under-steepened until the contact reaches the outlet. At this moment, another wave of incision (herein referred to as the outlet knickpoint) rapidly propagates upstream, bringing the profile to topographic steady state. The outlet knickpoint's celerity scales with K_f and consistently exceeds that of the uplift knickpoint (Fig. 11). If the duration of time between the change in uplift rate and exposure of the hard unit at the outlet is sufficiently short, the outlet knickpoint catches the uplift knickpoint. When this happens, the two waves merge, and the resulting knickpoint's

vertical velocity exceeds that of the uplift knickpoint prior to the merge by an amount that scales inversely with the hard unit's K (Fig. 12).

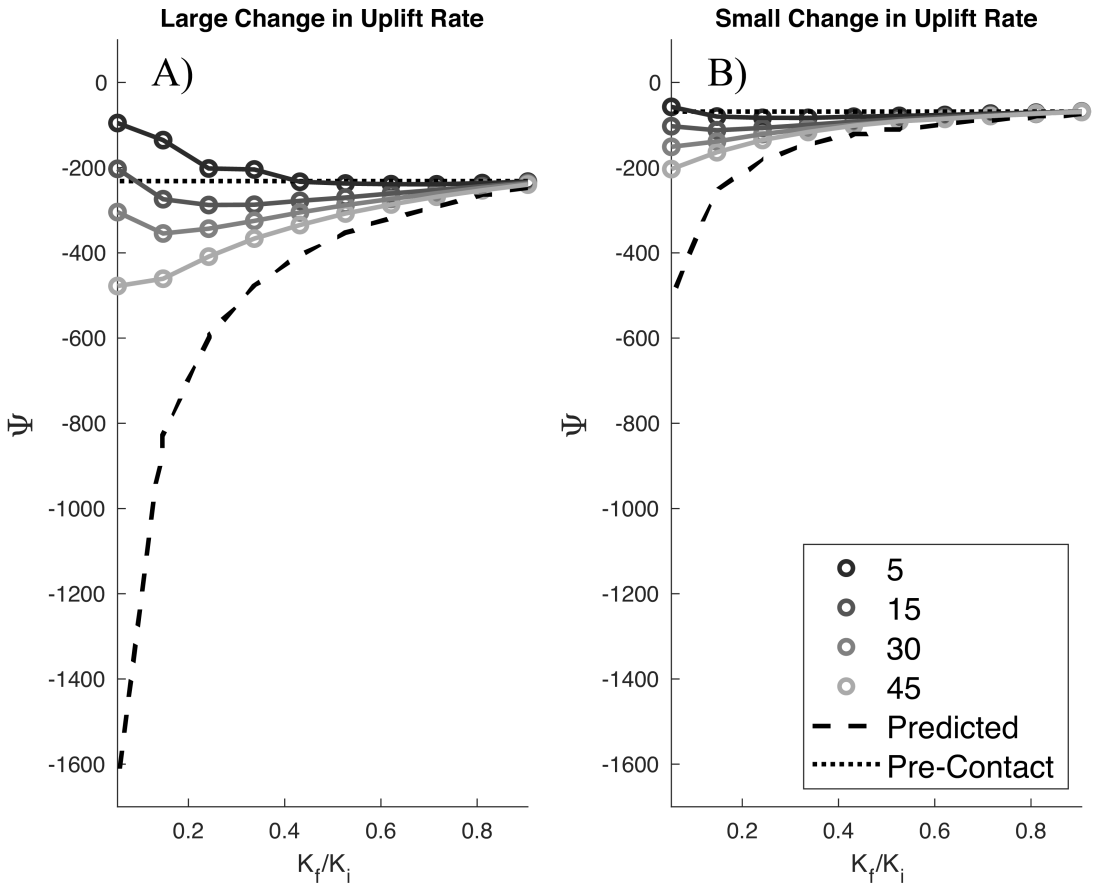

Fig. 10. Uplift knickpoint prominence after passing from a soft unit into a hard unit for varying K_f/K_i ratios and positive contact dip angles. The dashed lines show predicted prominence in the soft unit assuming topographic steady state, and the dotted lines show the knickpoint's prominence in the hard unit assuming topographic steady state.

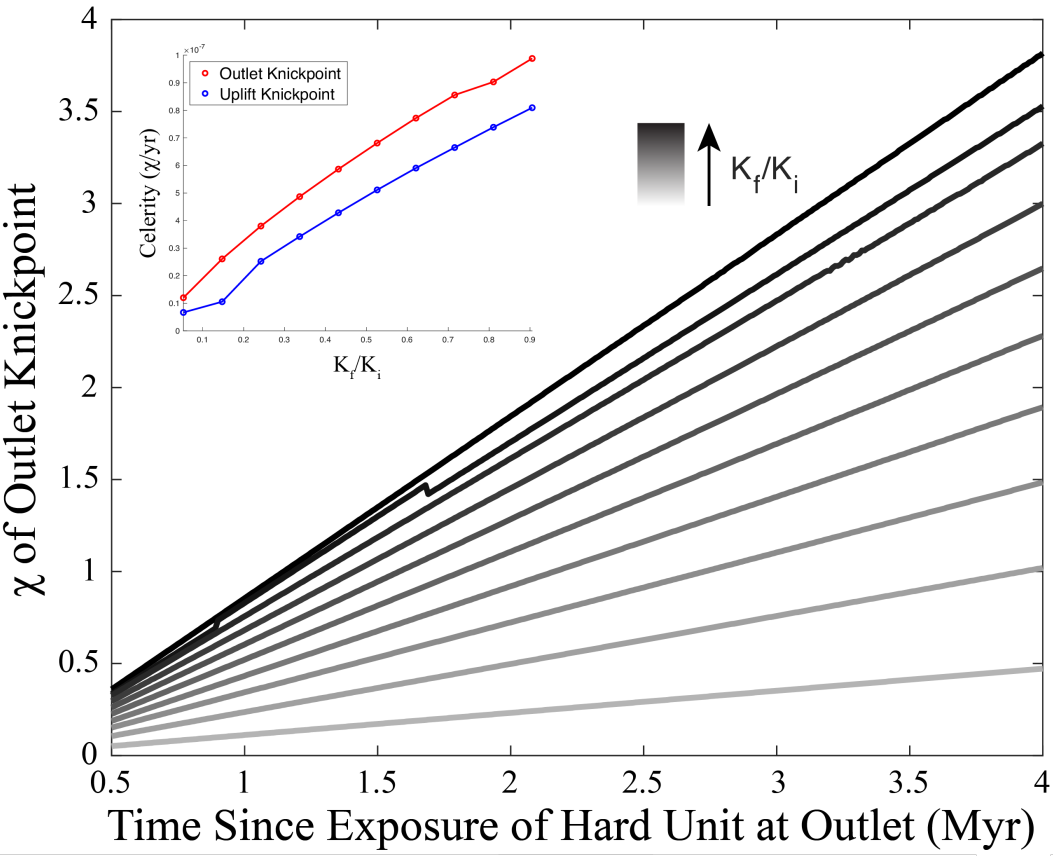

Fig. 11. χ distance from the stream's outlet of knickpoints formed after a hard unit is exposed at the outlet. Time is with respect to when the hard unit is first exposed at the outlet. All model runs have a contact dipping 5 degrees towards the outlet and soft over hard stratigraphy. The uplift knickpoint is generated by a change in uplift rate from 5×10^{-5} m/yr to 2.5×10^{-4} m/yr. The inset plot shows celerity in χ-space of the outlet knickpoint and uplift knickpoint with respect to the K_f/K_i ratio for the same runs used to produce the large plot.

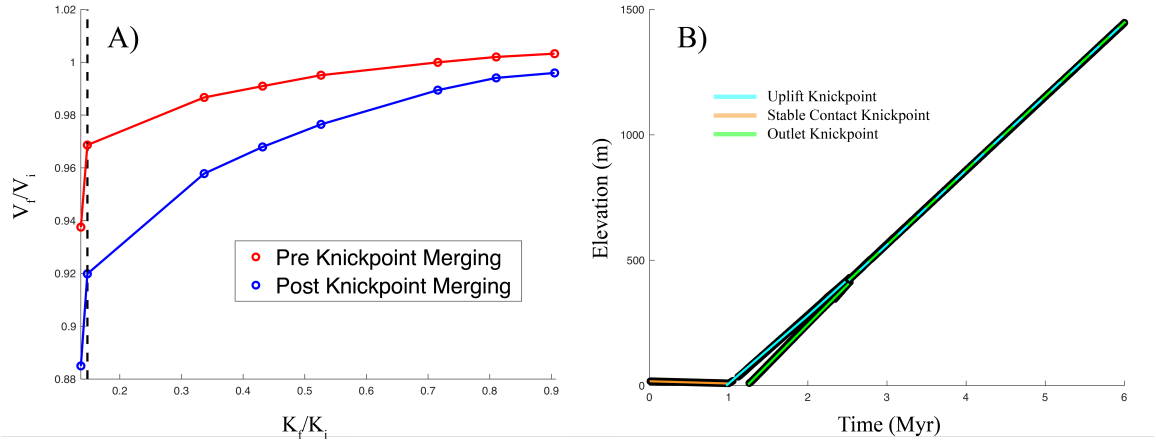

Fig. 12. Normalized vertical velocity of uplift knickpoints before and after merging with contact knickpoints generated by the exposure of a hard unit of various K values at the outlet with a 5° contact dip (A). Panel (B) shows a time-elevation plot of knickpoints throughout a run represented by the dashed black line in panel (A). Note that the outlet knickpoint merges with the uplift knickpoint after they intersect.

4.2. Hard Over Soft Contacts with Positive Dips

Depending on the stream's relief relative to the contact's dip, the contact is first exposed either at the stream's head or somewhere in its interior. As the contact migrates downstream, k_{sn} in the soft unit upstream from the contact decreases but remains over-steepened. Additionally, k_{sn} slowly increases when moving from the contact to stream head. The degree of over-steepening in the soft unit scales as the soft unit's K increases and contacts shallow. For runs with steeper contact dips, discrete waves that become more subtle over time become notable features in $\chi - k_{sn}$ space. Their magnitudes and celerities increase with the soft unit's K, and their wavelengths increase as contact dip steepens. k_{sn} gradually decreases in the wake of these waves as they propagate upstream (Fig. 13).

Once in the soft unit, an uplift knickpoint's vertical velocity increases as the soft unit's K increases and contact dips approach horizontal (Fig. 14). The relations between the soft unit's K and knickpoint vertical velocity are well described by power law fits when dips are 5° and 15°, with changes in K mainly causing changes in power law exponents. At

steeper dips, the knickpoint vertical velocities are more scattered and remain near the predicted analytical value. Exponential fits more accurately describe the relations between contact dip and knickpoint vertical velocity for small uplift rate scenarios, while power law fits remain more accurate for large uplift rate scenarios, though the scattered data at steep contact dips prevent strong trends from emerging from these fits. The reach downstream from the uplift knickpoint and upstream from the contact remains over-steepened, with the degree of over-steepening increasing as the soft unit's K increases and contact dip

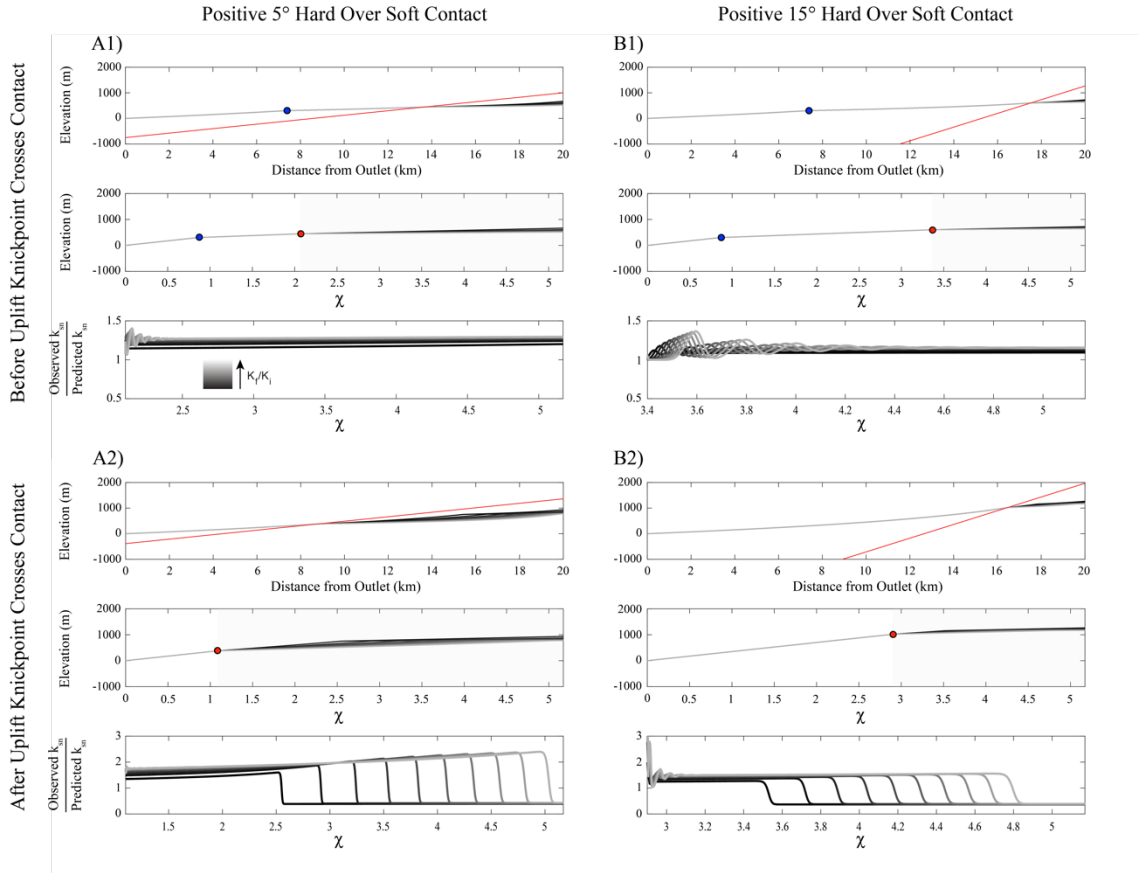

Fig. 13. Model runs with hard over soft 5° (A1 and A2) and 15° (B1 and B2) dips with K_f/K_i ratios ranging from 2.8 to 19 before (A1 and B1) and after (A2 and B2) an uplift knickpoint crosses a contact. A1 and B1 are 1 Myr after uplift rate is changed from 5×10^{-5} m/yr to 2.5×10^{-4} m/yr. A2 is 2.45 Myr after the change in uplift rate, and B2 is 3.8 Myr after the change in uplift rate. The red lines are contacts in normal space, and the red dots are contacts in χ-space. The blue dots are uplift knickpoints. The shaded regions in χ-space are the lateral extent of the underlying plots of predicted vs. observed k_{sn}.

shallows. For runs with 5° dips, k_{sn} also gradually increases when moving from the contact to uplift knickpoint. Regardless of the change in uplift rate, shallow dips (15 degrees or less) with modest K_f/K_i ratios can drive knickpoints hundreds of meters higher than steady state analytical predictions over the course of several Myr, while dips of 30 or 45 degrees have a far lesser influence on the knickpoint's elevation through time.

Large Change in Uplift Rate

V_f/V_i Power Law Fits

Dip	Coeff.	Exp.	RMSE
5	3.08×10^{-4}	7.05×10^{-2}	1.02×10^{-6}
15	3.09×10^{-4}	2.68×10^{-2}	2.42×10^{-6}
30	3.09×10^{-4}	6.47×10^{-3}	3.22×10^{-6}
45	2.92×10^{-4}	2.92×10^{-2}	5.19×10^{-6}

Small Change in Uplift Rate

V_f/V_i Power Law Fits

Dip	Coeff.	Exp.	RMSE
5	1.41×10^{-4}	2.87×10^{-2}	7.13×10^{-7}
15	1.40×10^{-4}	1.08×10^{-2}	1.22×10^{-6}
30	1.41×10^{-4}	-1.04×10^{-3}	3.83×10^{-6}
45	1.37×10^{-4}	-2.38×10^{-2}	8.62×10^{-6}

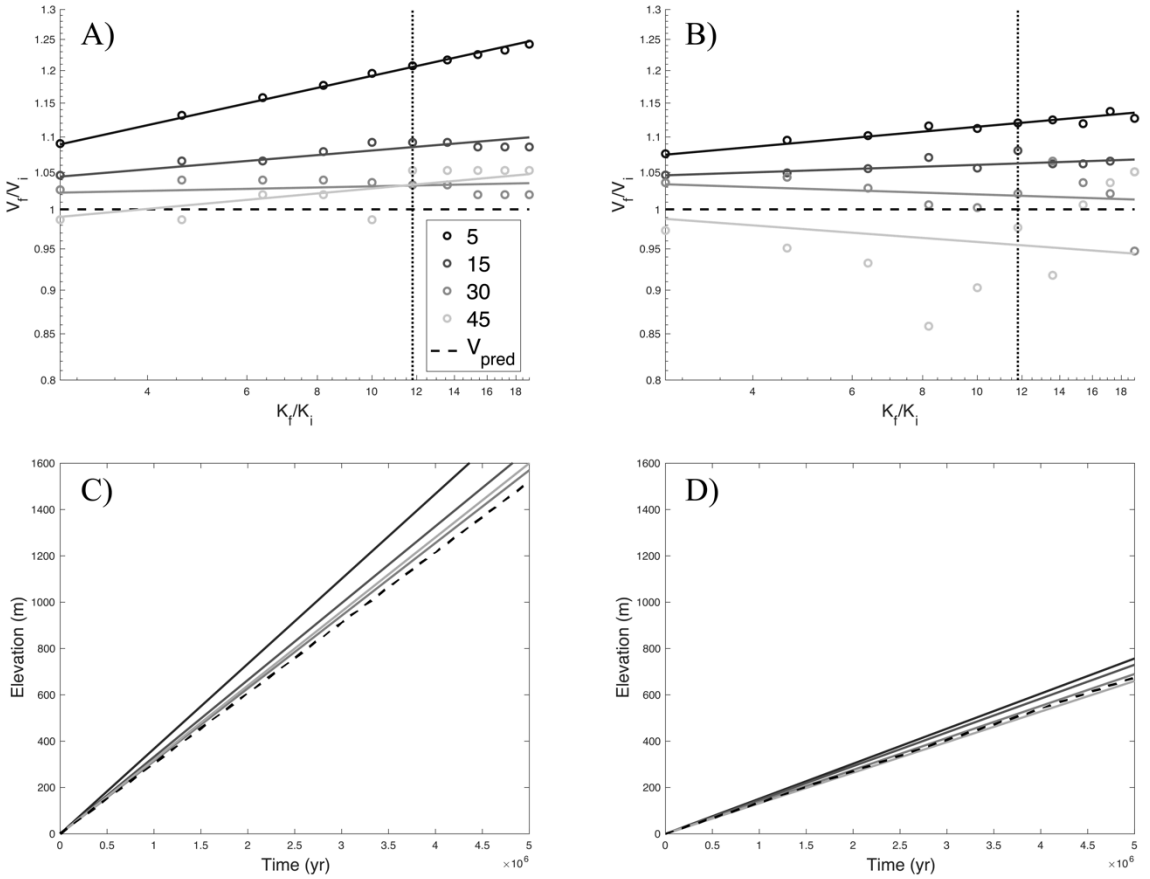

Fig. 14. Influence of the K_f/K_i ratio and contact dip on the vertical velocity of uplift knickpoints after passing hard over soft contacts with positive dips (panels A and B). Panels C and D show time series of uplift knickpoint elevations after passing contacts with varying dips and K_f/K_i ratios equal to 11.8 (dashed vertical lines in panels A and B). In

panels C and D, time 0 occurs immediately after uplift knickpoints pass a contact, and elevations are measured with respect to the knickpoint's elevation at time 0.

After entering the soft unit, the uplift knickpoint decreases prominence but remains more prominent than the predicted steady state value (Fig. 15). When holding contact dip angle and the K_f/K_i ratio fixed, increasing the change in uplift rate causes a greater deviation between the observed and predicted knickpoint prominence. For runs with steeply dipping contacts and small changes in uplift rate, the knickpoint's prominence is

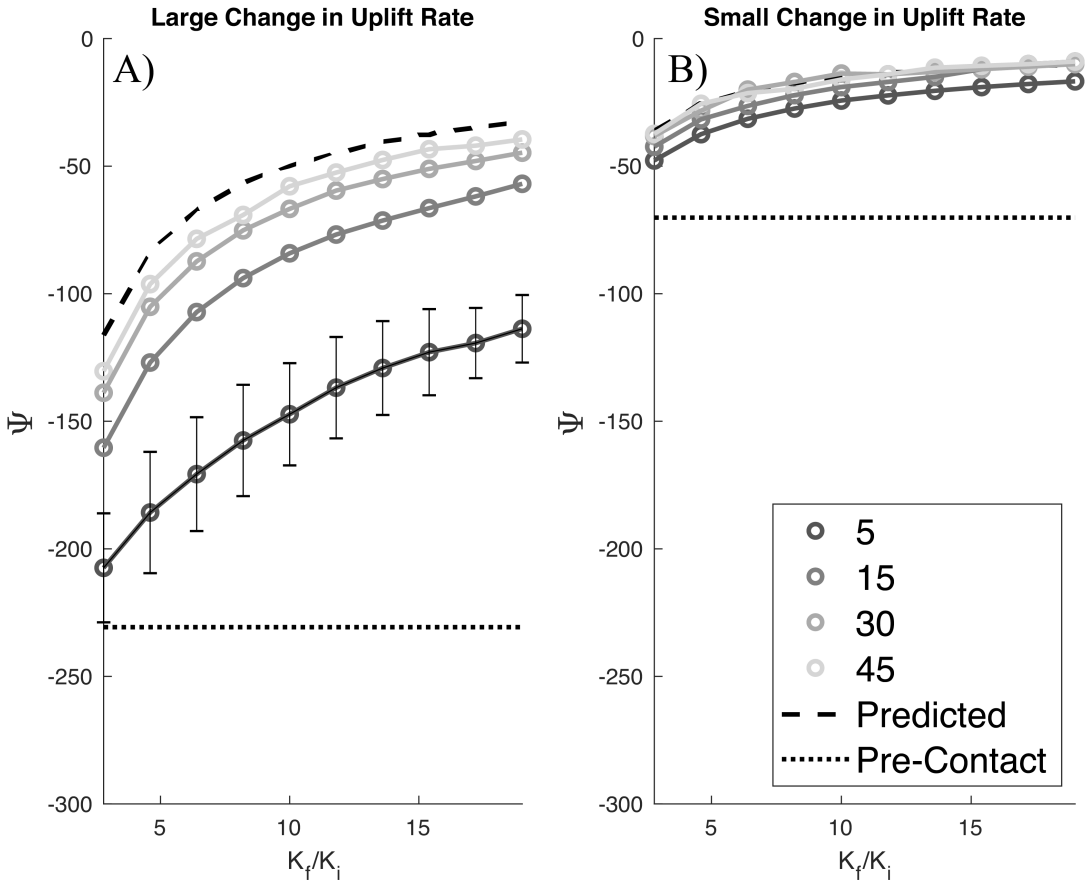

Fig. 15. Uplift knickpoint prominence after passing from a hard unit into a soft unit for varying K_f/K_i ratios and positive contact dip angles. The dashed lines show predicted prominence in the soft unit assuming topographic steady state, and the dotted lines show the knickpoint's prominence in the hard unit assuming topographic steady state. Error bars are included for the 5° contact dip scenarios because knickpoint prominence significantly decreases in the soft unit as these runs progress.

approximately the predicted value. However, when the change in uplift rate is large, even 45° contacts cause a notable deviation between the observed and predicted knickpoint prominence, and this deviation increases as contact dips shallow. As is predicted when assuming topographic steady state, prominence in the soft unit also increases nonlinearly as the K_f/K_i ratio approaches 1. In the soft unit, the uplift knickpoint's prominence in most runs is either constant or nearly constant and decreases at an extremely slow rate. For most contact dip angles, this small decline in prominence is on the order of a few units and only notable for runs with relatively low erodibility soft units. However, when contact dip is 5°, prominence decreases significantly (by at least 25 units) as the knickpoint propagates through the soft rock, and the amount by which prominence in the soft unit decreases scales with the soft unit's K.

As with the soft over hard positively dipping contact runs, the reach upstream from the contact remains over-steepened until the contact reaches the outlet. An outlet knickpoint then sweeps upstream, lowering k_{sn} to steady state. When the outlet knickpoint reaches the uplift knickpoint, the two incisional waves merge. If the underlying soft unit is relatively hard (K_f/K_i ratio near 1), the resulting wave has a lower, albeit marginally so, vertical velocity than the uplift knickpoint prior to the merge. However, as the soft unit's K increases, the influence of the outlet knickpoint on the vertical velocity of the uplift knickpoint becomes negligible (Fig. 16).

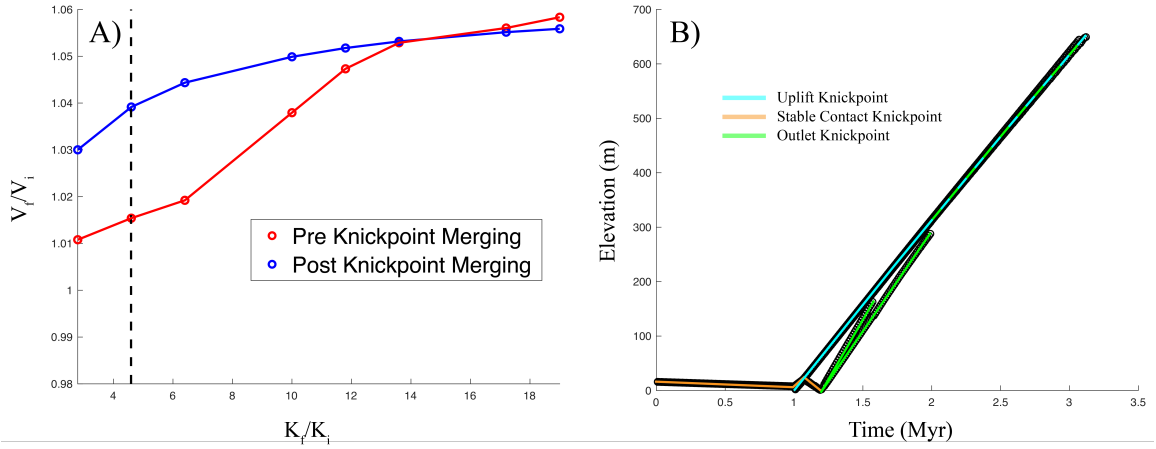

Fig. 16. Normalized vertical velocity of uplift knickpoints before and after merging with contact knickpoints generated by the exposure of a soft unit of various K values at the outlet with a 5° contact dip (A). Panel (B) shows a time-elevation plot of knickpoints throughout a run represented by the dashed black line in panel (A). Note that the outlet knickpoint merges with the uplift knickpoint after they intersect.

4.3. Soft Over Hard Contacts with Negative Dips

The contact's first exposure at the outlet induces a transient contact knickpoint to propagate upstream ahead of the contact with a celerity that scales with the soft unit's K. This wave reduces k_{sn} in its wake to below topographic steady state. The profile's k_{sn} decreases more as contact dip approaches horizontal and, to a far lesser degree, as the soft unit's K increases (Fig. 17). Unlike the stable contact knickpoint, the transient contact knickpoint is a subtle feature along the profile, and its prominence decreases as the contact's dip steepens such that it is virtually undetectable in χ-space for runs with a 45° contact dip. For runs with shallower contact dips, this wave forms a smooth concave reach upstream from the contact in χ-space (Fig. 17). The profile downstream from the contact stays at steady state k_{sn}.

Uplift knickpoints decrease vertical velocity upon propagating into the soft unit (Fig. 18). While the uplift knickpoint increases k_{sn} in its wake, the reach downstream from the uplift knickpoint and upstream from the contact remains under-steepened. The

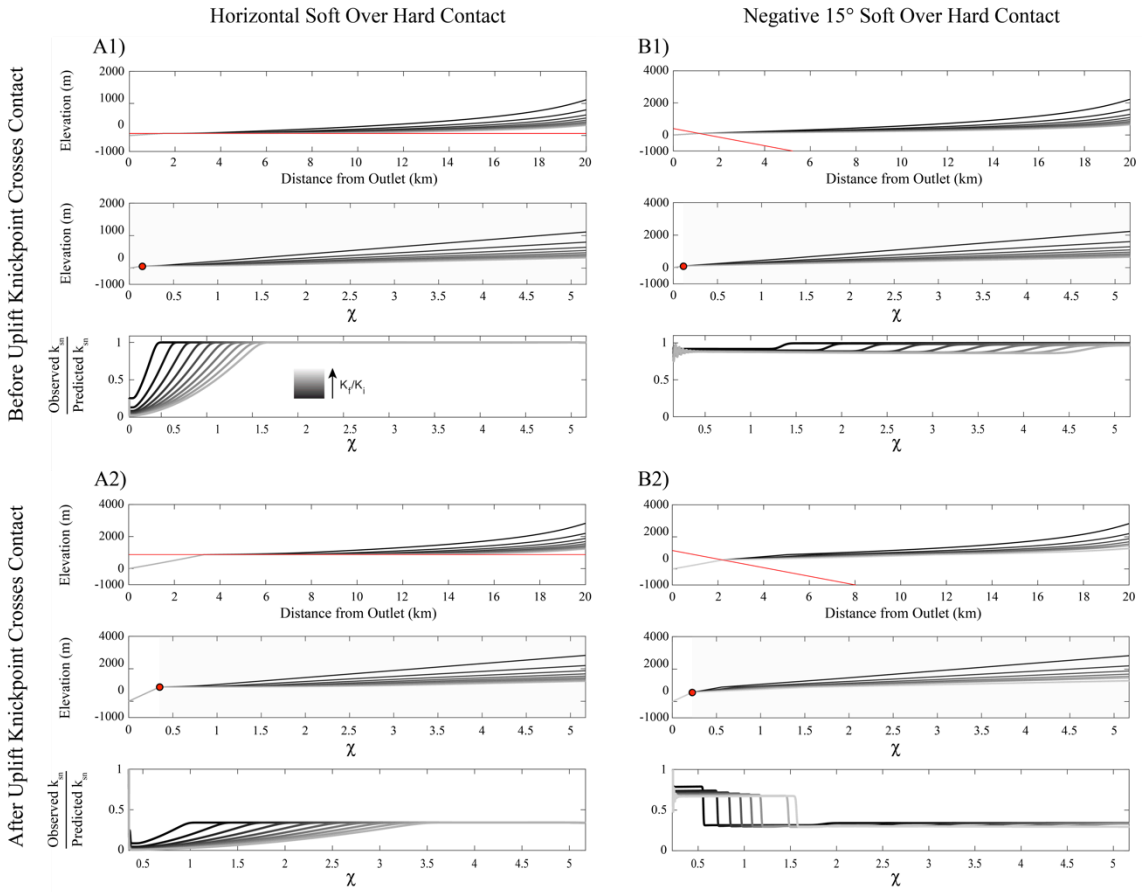

Fig. 17. Model runs with soft over hard horizontal (A1 and A2) and -15° (B1 and B2) dips and K_f/K_i ratios ranging from 2.8 to 19 before (A1 and B1) and after (A2 and B2) an uplift knickpoint crosses a contact. A1 and B1 are prior to a change in uplift rate from $5\text{x}10^{-5}$ m/yr to $2.5\text{x}10^{-4}$ m/yr. A2 and B2 are 3 Myr after the change in uplift rate. The red lines are the contacts in regular space, and the red dots are the contacts in χ-space. The shaded regions in χ-space are the lateral extent of the underlying plots of the ratio of observed to predicted k_{sn}.

relationship between contact dip and uplift knickpoint 's change in vertical velocity is well explained by a power law fit, with the power law coefficient decreasing and exponent increasing as the K_f/K_i ratio increases. When holding contact dip constant and varying the K_f/K_i ratio, the uplift knickpoint's change in vertical velocity is also well described by a power law relationship, with the coefficient increasing and exponent decreasing as the soft unit's K increases. Over the course of several million years, the reduction in knickpoint vertical velocity caused by a near horizontal soft over hard contact with K values differing

by an order of magnitude can drive knickpoint elevations several hundred meters lower than would be predicted under steady state topography (Fig. 18).

For runs with a horizontal contact dip, the transient contact knickpoint outpaces the uplift knickpoint, and the two waves never interact. However, when contact dips are

Large Change in Uplift Rate

V_f/V_i Power Law Fits

Dip	Coeff.	Exp.	RMSE
0	2.74×10^{-4}	-2.69×10^{-2}	4.71×10^{-6}
5	2.88×10^{-4}	-2.32×10^{-2}	1.04×10^{-6}
15	2.97×10^{-4}	-1.34×10^{-2}	8.00×10^{-7}
30	3.01×10^{-4}	-6.43×10^{-3}	4.06×10^{-7}
45	3.02×10^{-4}	-3.37×10^{-3}	3.29×10^{-7}

Small Change in Uplift Rate

V_f/V_i Power Law Fits

Dip	Coeff.	Exp.	RMSE
0	1.08×10^{-4}	-3.18×10^{-2}	1.10×10^{-6}
5	1.26×10^{-4}	-3.04×10^{-2}	7.13×10^{-7}
15	1.33×10^{-4}	-1.90×10^{-2}	2.41×10^{-7}
30	1.34×10^{-4}	-1.04×10^{-2}	2.00×10^{-7}
45	1.35×10^{-4}	-6.84×10^{-3}	2.84×10^{-7}

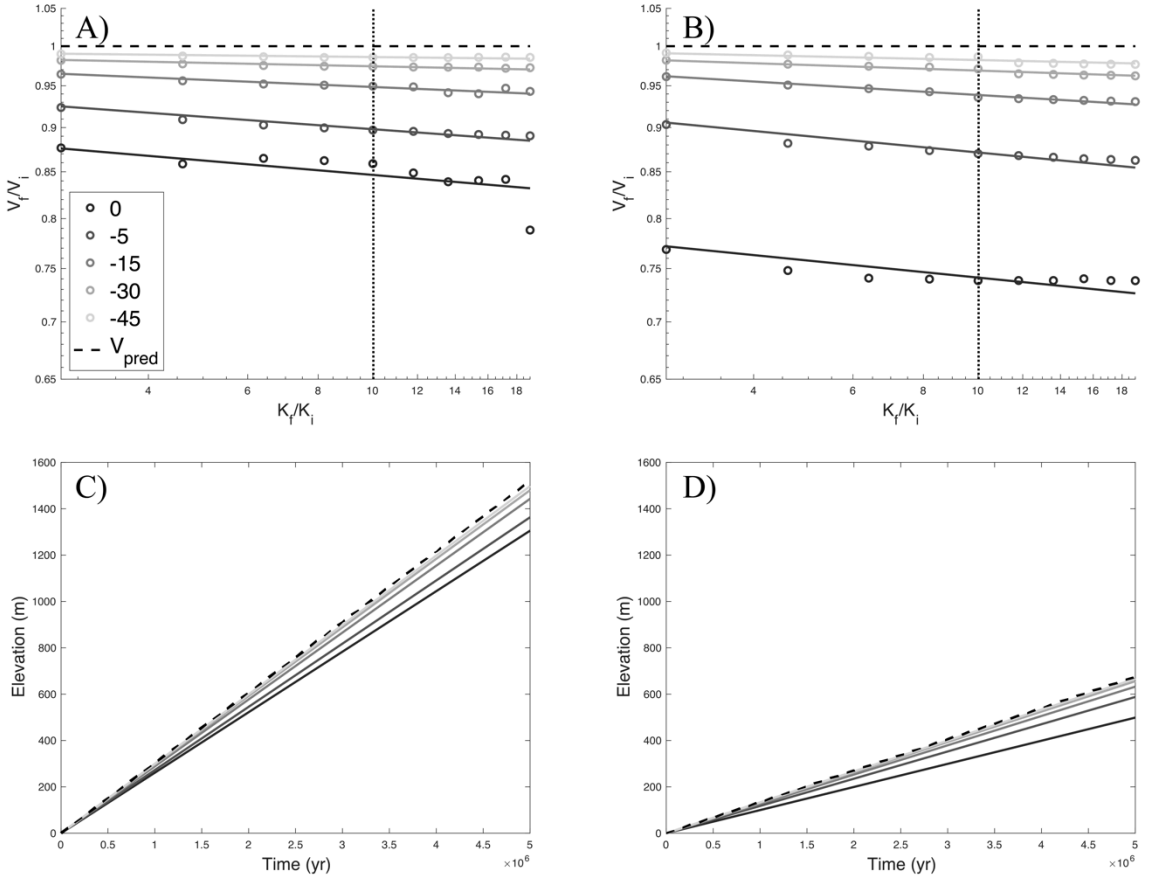

Fig. 18. Influence of the K_f/K_i ratio and contact dip on the vertical velocity of uplift knickpoints after passing soft over hard contacts with horizontal or negative dips (panels A and B). Panels C and D show time series of uplift knickpoint elevations after passing contacts with varying dips and K_f/K_i ratios equal to 10 (dashed vertical lines in panels A and B). In panels C and D, time 0 occurs immediately after uplift knickpoints pass a contact, and elevations are measured with respect to the knickpoint's elevation at time 0.

sufficiently steep, the uplift knickpoint catches the transient contact knickpoint, and the two waves merge. Knickpoint time series do not suggest a clear change in vertical velocity after this merge, and the measured changes in vertical velocity are minor, amounting to deviations in uplift knickpoint elevations from steady state predictions of no greater than 2.5 meters per million years (Fig. 19).

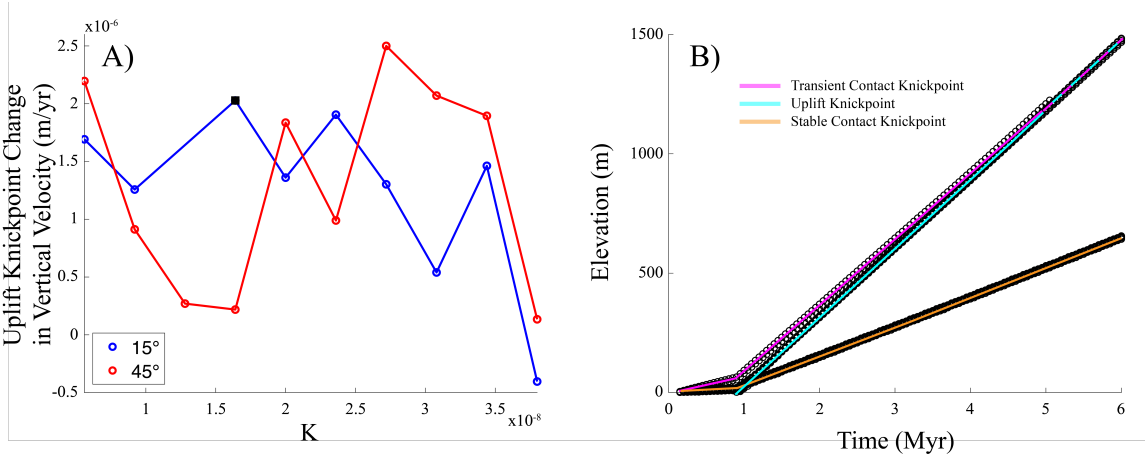

Fig. 19. Changes in uplift knickpoint vertical velocities after merging with transient contact knickpoints for runs with soft over hard stratigraphy (A) and time series for a run with a soft unit K equal to 1.64x10^{-8} m$^{-0.5}$yr^{-1} and 15° contact dip (B). The run that generated panel (B) is represented by a black square in panel (A). Uplift knickpoints were generated by a uniform change in uplift rate from 5x10^{-5} m/yr to 2.5x10^{-4} m/yr.

After propagating into the softer unit, the uplift knickpoint's prominence decreases, and k_{sn} upstream of the contact and downstream from the uplift knickpoint remains under-steepened. The uplift knickpoint's prominence in the soft unit is also consistently below that of the predicted value and further deviates from the predicted values as the contact dip approaches horizontal and the soft unit's K decreases (Fig. 20).

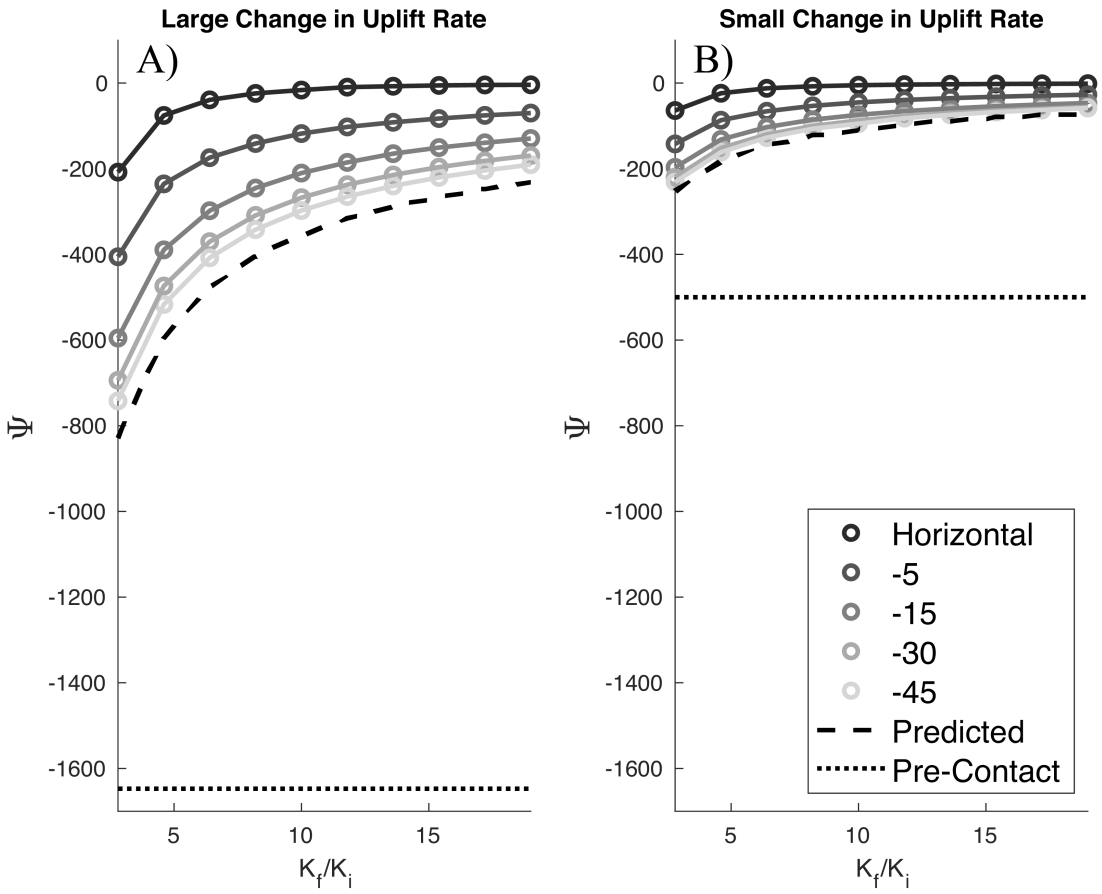

Fig. 20. Uplift knickpoint prominence after passing from a hard unit into a soft unit for varying K_f/K_i ratios and horizontal and negative contact dips. The dashed lines show predicted prominence in the soft unit assuming topographic steady state, and the dotted lines show the knickpoint's prominence in the hard unit.

4.4. Hard Over Soft Contacts with Negative Dips

Again, the exposure of a horizontal or negatively dipping contact at the stream's outlet produces a transient contact knickpoint that increases upstream celerity with the hard unit's K. As the contact approaches horizontal and the K_f/K_i ratio decreases from 1, the contact's celerity increases with respect to the transient contact knickpoint. Since the contact cannot undercut the transient contact knickpoint, shallower dips and harder hard units produce a more over-steepened reach between the contact and transient contact knickpoint. For runs with the lowest tested hard unit K values and horizontal contacts, the

over-steepened reach begins just downstream of the contact, while for other runs, the over-steepened reach exclusively resides within the hard unit. For runs with steeper contacts and softer hard units, the transient contact kickpoint becomes a finer detail along the stream's profile, and it is hardly detectable in χ-space when dips exceed -15°, regardless of the hard unit's K value. Upstream of the transient contact knickpoint's wave front, the stream remains at topographic steady state prior to a change in uplift rate (Fig. 21).

For most of the model runs with negatively dipping hard over soft contacts, uplift

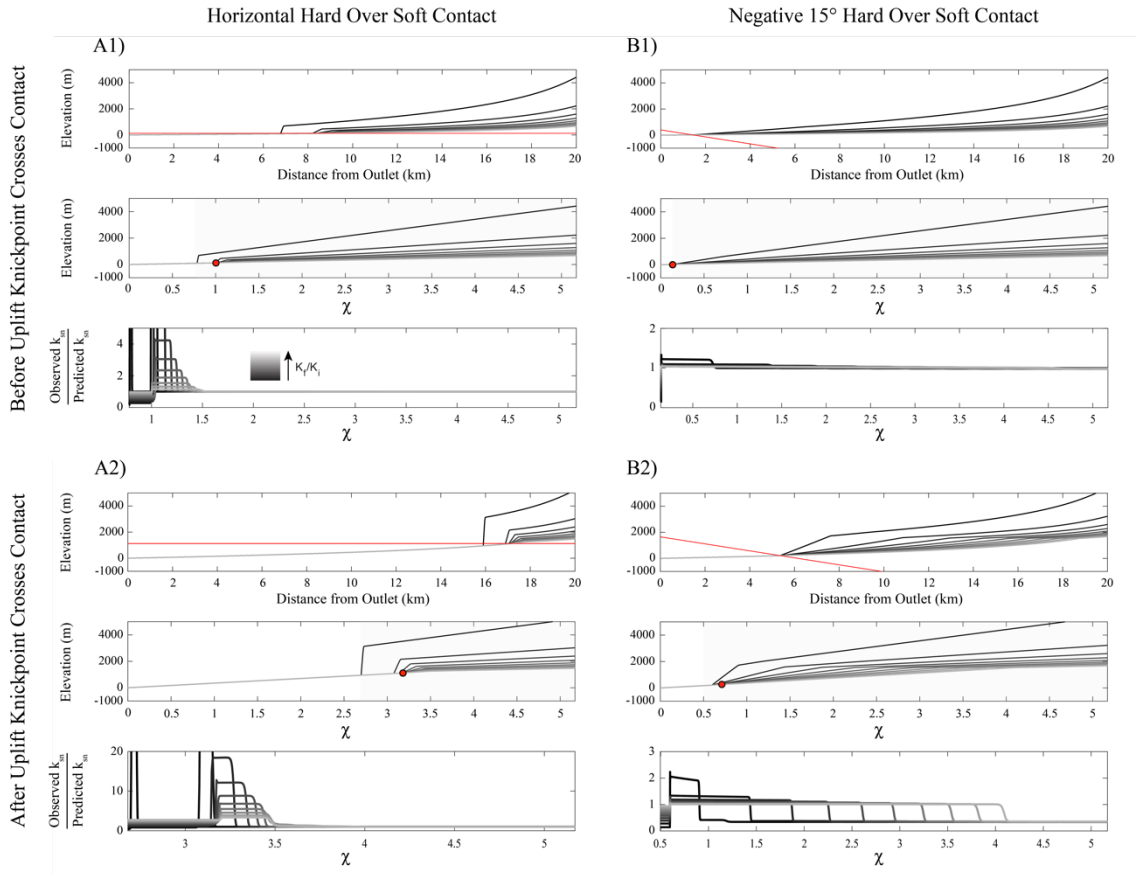

Fig. 21. Model runs with hard over soft horizontal (A1 and A2) and -5° (B1 and B2) dips with K_f/K_i ratios ranging from 0.05 to 0.91 before (A1 and B1) and after (A2 and B2) an uplift knickpoint crosses a contact. A1 and B1 are before uplift rate is changed from 5×10^{-5} m/yr to 2.5×10^{-4} m/yr. A2 is 4 Myr after the change in uplift rate, and B2 is 5 Myr after the change in uplift rate. The red lines are contacts in normal space, and the red dots are contacts in χ-space. The shaded regions in χ-space are the lateral extent of the underlying plots of predicted vs. observed k_{sn}.

knickpoints increase vertical velocity after propagating into the oversteepened reach between the contact and transient contact knickpoint (Fig. 22). Vertical velocities conform fairly well to power law fits with respect to both contact dips and the K_f/K_i ratio, such that

Large Change in Uplift Rate

V_f/V_i Power Law Fits

Dip	Coeff.	Exp.	RMSE
0	2.06×10^{-4}	-1.18	5.54×10^{-5}
5	2.56×10^{-4}	-0.26	3.10×10^{-5}
15	2.96×10^{-4}	-0.06	5.72×10^{-6}
30	3.02×10^{-4}	-0.02	2.02×10^{-6}
45	3.04×10^{-4}	-0.01	1.07×10^{-6}

Small Change in Uplift Rate

V_f/V_i Power Law Fits

Dip	Coeff.	Exp.	RMSE
0	1.04×10^{-4}	-1.28	1.36×10^{-5}
5	1.18×10^{-4}	-0.23	1.17×10^{-5}
15	1.33×10^{-4}	-0.05	2.21×10^{-6}
30	1.35×10^{-4}	-0.02	1.03×10^{-6}
45	1.35×10^{-4}	-0.02	1.13×10^{-6}

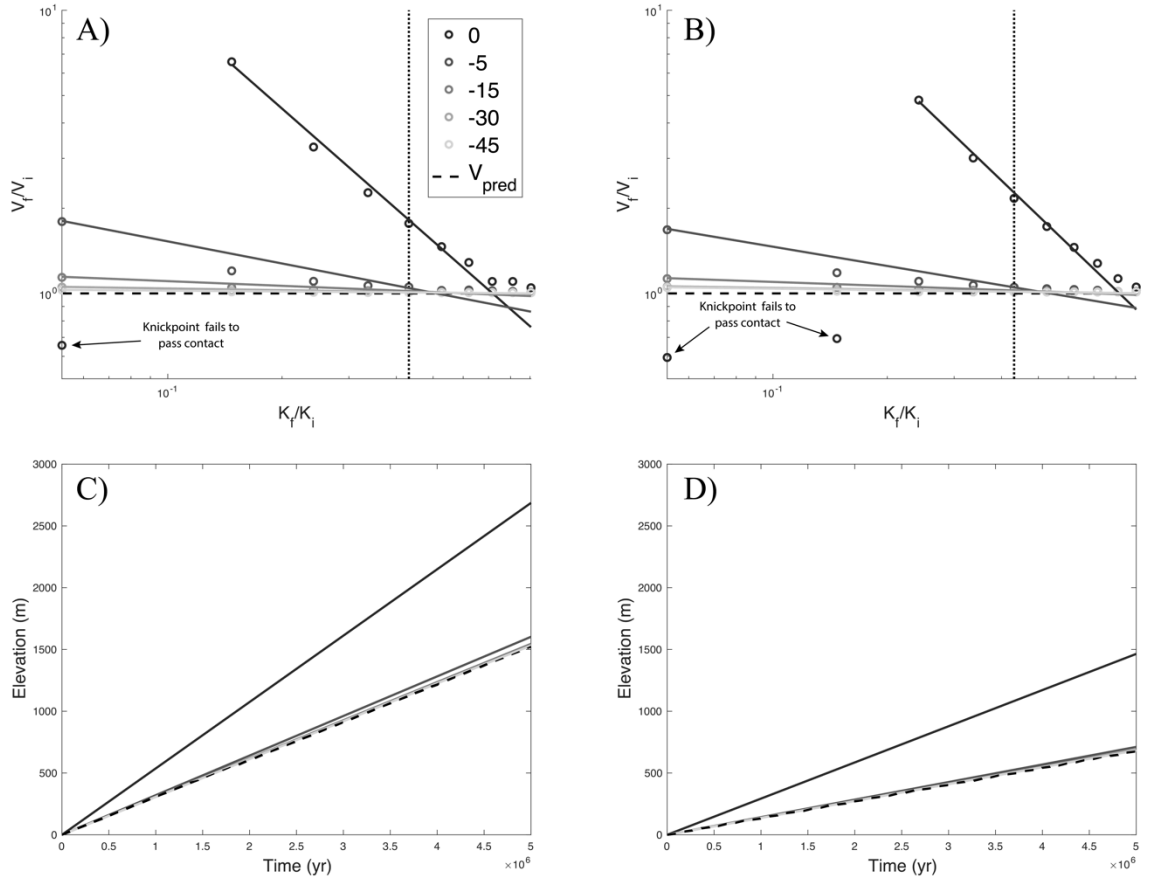

Fig. 22. Influence of the K_f/K_i ratio and contact dip on the vertical velocity of uplift knickpoints in the hard unit's reach upstream from the contact but downstream from the transient contact knickpoint (panels A and B). Panels C and D show time series of uplift knickpoint elevations after passing contacts with varying dips and K_f/K_i ratios equal to 0.43 (dashed vertical lines in panels A and B). The velocities used to produce each plot are taken from within the oversteepened reach between the contact and transient contact knickpoint. In panels C and D, time 0 occurs immediately after uplift knickpoints pass a contact, and elevations are measured with respect to the knickpoint's elevation at time.

vertical velocities increase as dips approach horizontal and K_f/K_i ratios decrease from unity (Fig. 22). However, knickpoint vertical velocities upstream of contacts dipping steeper than -5° remain near the predicted values. When contact dip is sufficiently shallow and/or the hard unit's K value is sufficiently low, uplift knickpoints catch the transient contact knickpoint, and the two waves merge. The resulting knickpoint has a vertical velocity between that of the two knickpoints prior to the merge. Shallower dips and lower hard unit K values produce a more oversteeped reach between the contact and transient contact knickpoint, a greater uplift knicpoint vertical velocity in the oversteepened reach, and a greater change in uplift knickpoint vertical velocity upon merging with the transient contact knickpoint (Fig. 23). Of note, uplift knickpoints are not detected in the oversteepened reach when contact dips are horizontal and the hard unit's K is sufficiently low (Fig. 22A-B). The threshold hard unit K required for the uplift knickpoint to not propagate past the contact scales inversely with the change in uplift rate. For runs in which the uplift knickpoint is not detected in the over-steepened reach, the transient contact knickpoint still increases vertical velocity after the uplift knickpoint reaches the contact. This mimics the behavior of the merged uplift/transient contact knickpoint and suggests that the uplift knickpoint may propagate through the oversteepened reach to merge with the transient contact knickpoint despite being less detectable (Fig. 23). Aside from the horizontal contact case, trends and values in the V_f/V_i ratios for respective contacts appear independent of the change in uplift rate (Fig. 22).

Uplift knickpoints increase prominence when propagating into the hard unit (Fig. 24). As predicted assuming steady state topography, knickpoint prominence increases exponentially as the hard unit's K decreases. However, in the model runs, the knickpoint's

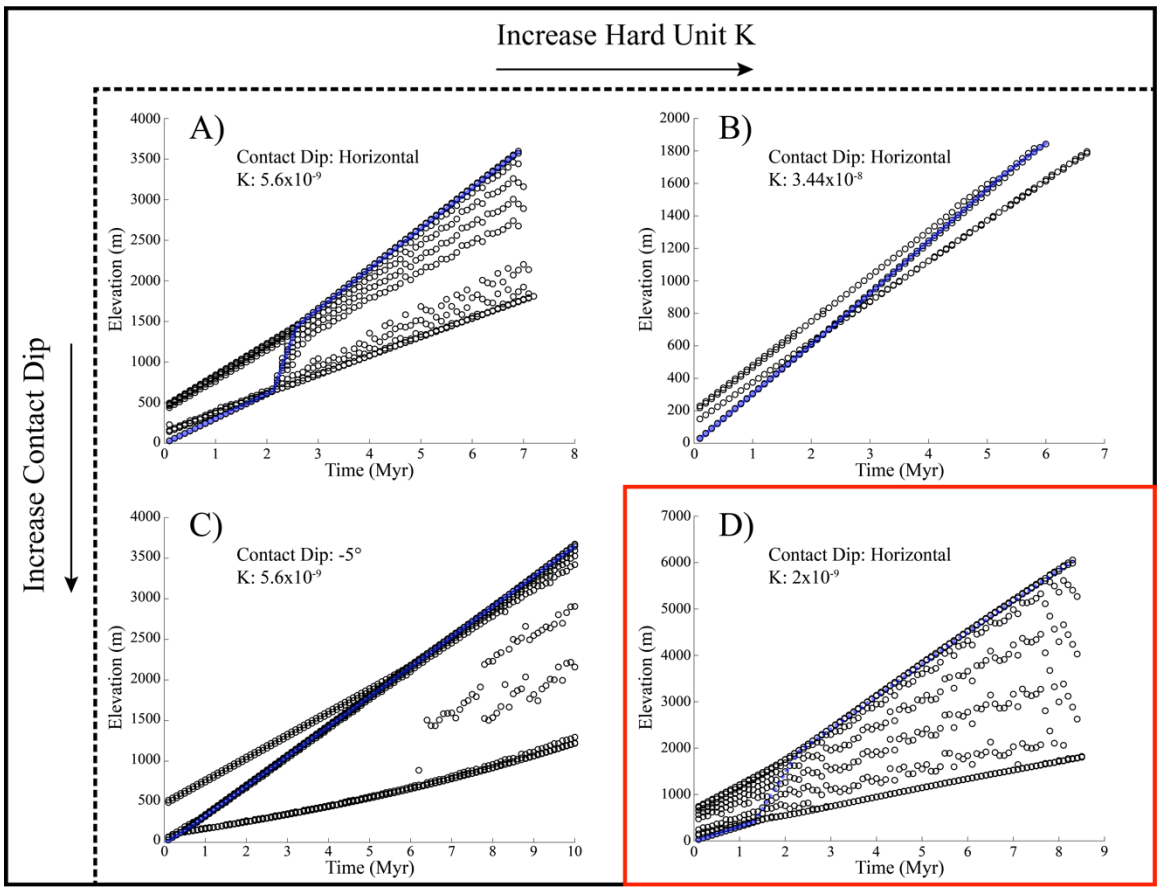

Fig. 23. Time-elevation plots of knickpoints in runs with a hard over soft negatively dipping contact showing the uplift knickpoint (blue tracing) merging with the transient contact knickpoint for various contact dips and hard unit K values (A-C). Panel (D) shows a run where the knickpoint is not clearly defined after interacting with the contact. The inferred path of the knickpoint beyond the contact is traced in dashed blue.

prominence consistently exceeds the predicted steady state value, and the deviation from the predicted value increases as the contact dip shallows. For a given contact dip angle, the deviation between the predicted and observed knickpoint prominence also increases as the hard unit's K decreases. Of note, when contact dips fail to exceed -15°, the uplift knickpoint forms a sharp peak in k_{sn} within a greatly over-steepened reach upstream of the contact, and its prominence cannot be accurately measured.

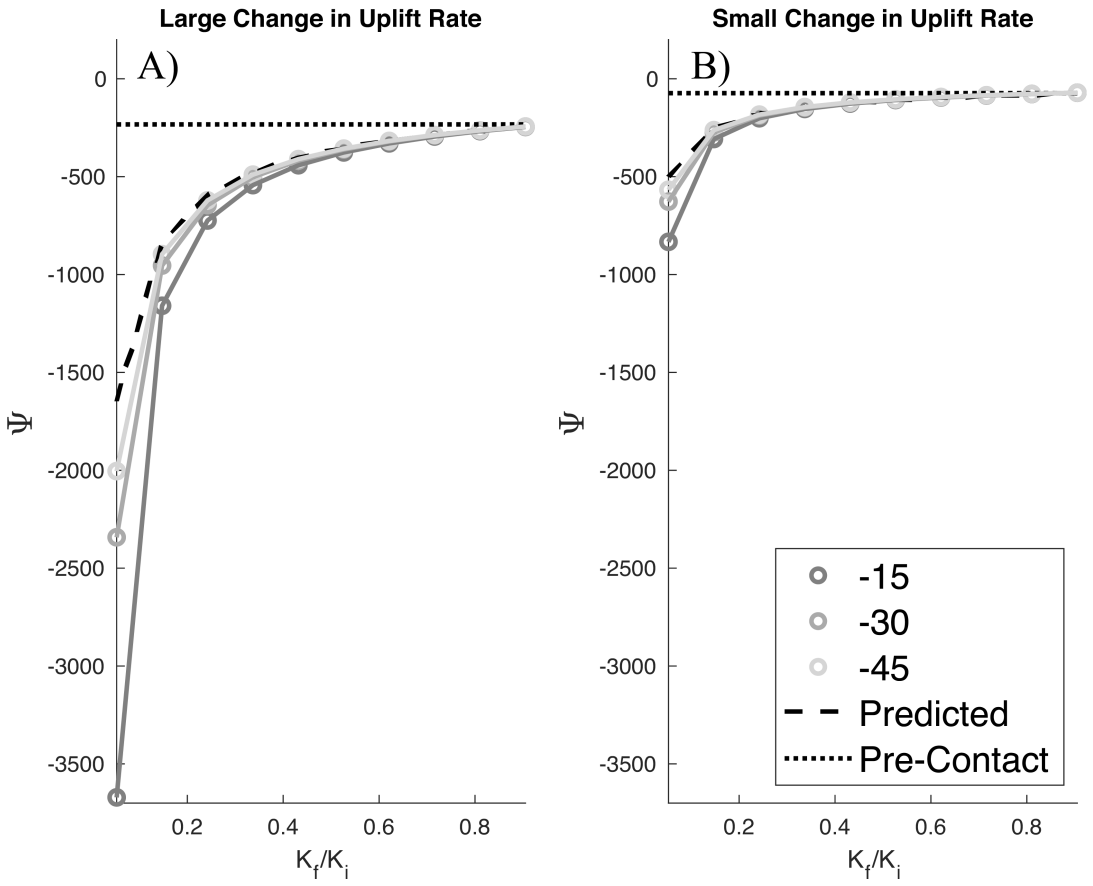

Fig. 24. Uplift knickpoint prominence after passing from a soft unit into a hard unit for varying K_f/K_i ratios and negative contact dips. Solid lines are interpolations. The dashed lines show predicted prominence in the hard unit assuming topographic steady state, and the dotted lines show the knickpoint's prominence in the soft unit.

5. Discussion

5.1. Baseline Single Contact Runs

The baseline runs suggest that non-vertical contacts drive deviations between observed and predicted uplift knickpoint behavior. Therefore, the discussion begins by describing how profiles evolve in response to the exposure of a non-vertical contact, prior to a change in uplift rate. Following sections then address how these profile alterations influence uplift knickpoint vertical velocity, celerity, and prominence. Lastly, implications for topographic analysis are discussed.

5.1.1. Positively Dipping Contacts with Downstream Celerity

Consider the case of a soft over hard contact dipping towards the stream outlet. Now, consider two adjacent positions along the stream with Position (A) located just upstream from Position (B) (Fig. 25). When the contact's outcrop migrates past Position (A), erosive power (dictated by the local slope and drainage area) fails to keep pace with uplift rate. As a result, Position (A)'s elevation increases along with the slope between Position (A) and Position (B). If the contact's location along the stream were to remain constant, Position (A) would continue to rise until reaching a downstream slope enabling geomorphic work to match uplift rate. Position (A)'s rise perturbs the next upstream position by decreasing its downstream slope, which causes the upstream position to rise. This signal of the contact's presence (i.e., a transient contact knickpoint) propagates upstream, driving the upstream reach towards topographic steady state.

However, under uniform rock uplift rate, a non-vertical contact migrates upstream (for negative contact dips) or downstream (for positive contact dips). When the contact

resides immediately downstream from Position (A) but upstream from Position (B), Position (B) acts as a stable boundary condition for further upstream positions. Eventually,

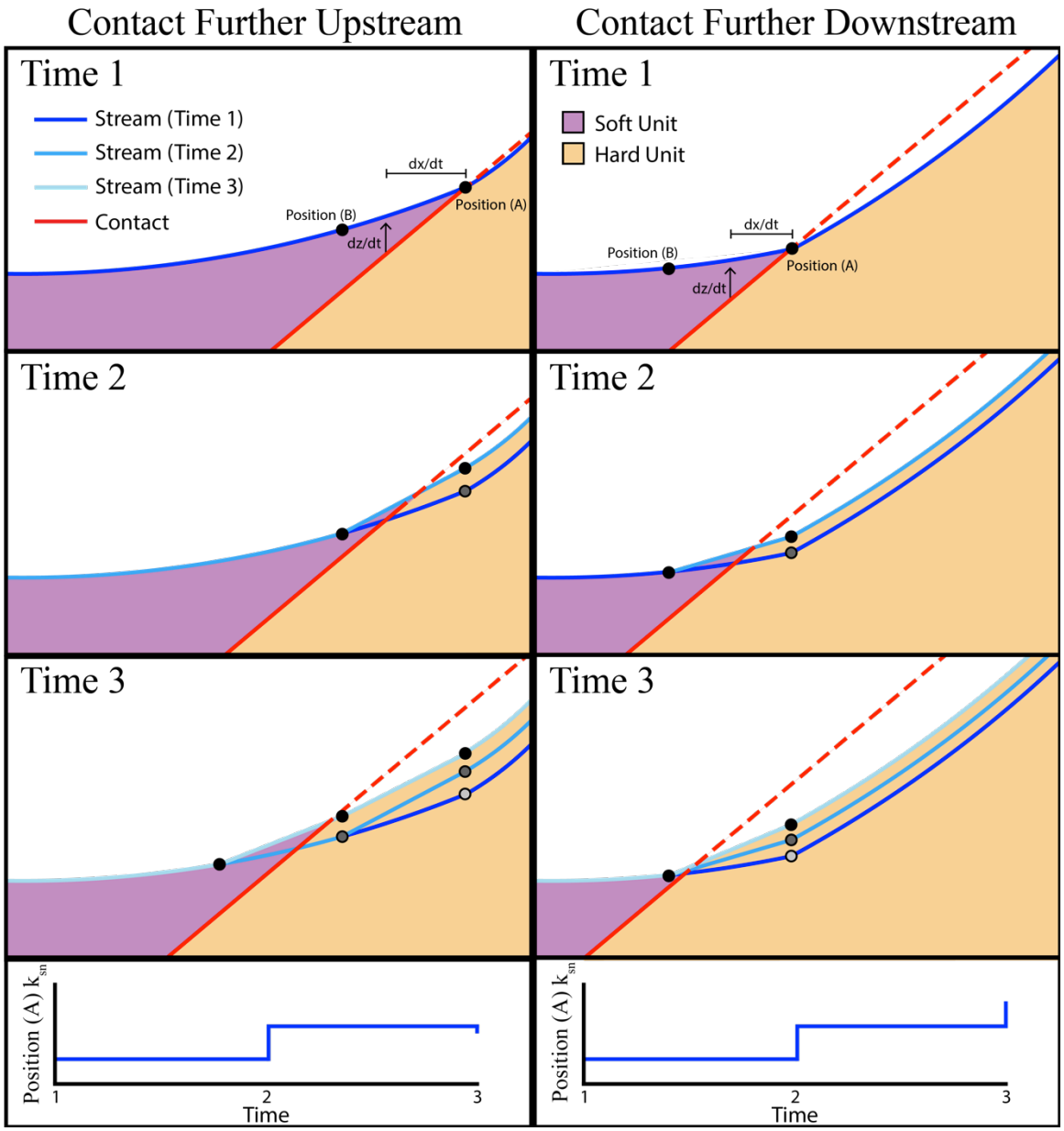

Fig. 25. Conceptual model (not to scale) outlining the cause and effect of a variable downstream contact migration rate on a stream with a positively dipping contact (red line) and soft (purple unit) over hard (orange unit) stratigraphy. Left panels show the contact's influence on an upstream (more steep) portion of the stream, while right panels show the contact's influence on a downstream (less steep) portion of the stream. The differing lengths of dx/dt in time 1 panels illustrates the spatially variable contact celerity along a concave profile, the effect of which is represented by time slices 2 and 3. Slopes between black dots (nodes) are depicted as straight lines (mimicking model behavior), while the profile outside of the discretized region resumes a smooth concave shape. Prior elevations

of Positions (A) and (B) are represented in time slices as progressively lighter-colored dots. The upstream and downstream scenarios share identical uplift rates that are constant through time and represented by vectors in the time 1 panels. The bottom panels show the evolutions of k_{sn} at position (A) for the Contact Further Upstream and Contact Further Downstream scenarios.

however, the contact migrates downstream of Position (B), instantaneously dropping its K, and prompting Position (B) to ascend towards a new equilibrium elevation. Yet, Position (A) does not equilibrate instantaneously. Rather, the rate at which Position (A) responds to transitioning to the hard unit decreases through time and is limited by the rock uplift rate (Fig. 26). Therefore, Position (A) remains under-steepened as the hard unit passes Position (B), whose initial rapid elevation rise briefly decreases Position (A)'s downstream slope (Fig. 27(A)). The rate at which Position (A) approaches its equilibrium k_{sn} then slows

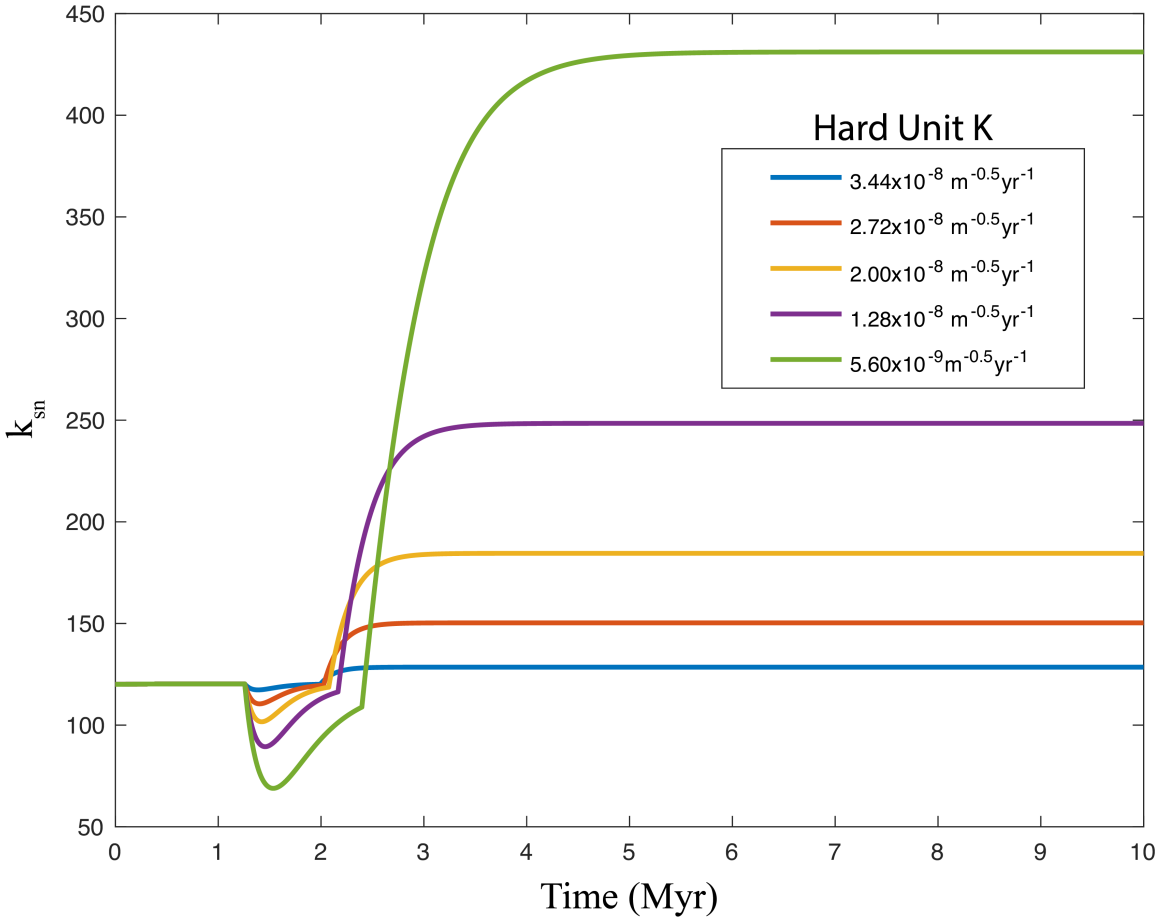

Fig. 26. Adjustments of k_{sn} in response to a change from a soft (K equal to 3.80x10^{-8} m$^{-0.5}$yr^{-1}) unit to a hard unit for varying hard unit K values. All runs have a constant uplift rate of 5x10^{-5} m/yr and a -15 degree dipping contact. Each curve shows k_{sn} at a node 20 m upstream from the outlet. Note that the rate of change in k_{sn} and duration of time needed for the node to reach its new equilibrium k_{sn} increases as the hard unit's K decreases.

significantly because, at each time step, Position (B) also rises. This process continues as the contact migrates downstream. Under-steepened positions upstream from the contact continue to rise, and kinematic waves generated while positions are immediately upstream from the contact propagate upstream as a chain of discrete pulses. When runs of identical contact dips but different K values are overlain, these pulses group together by the node at which they were generated, indicating that softer rocks yield waves of greater magnitude and celerity in χ-space (Fig. 13(A1 and B1)). If a transient contact knickpoint generated by a rise to a particular k_{sn} interacts with a position of a lower k_{sn}, the position of the lower k_{sn} steepens. The opposite occurs when a wave generated by a fall in k_{sn} interacts with an

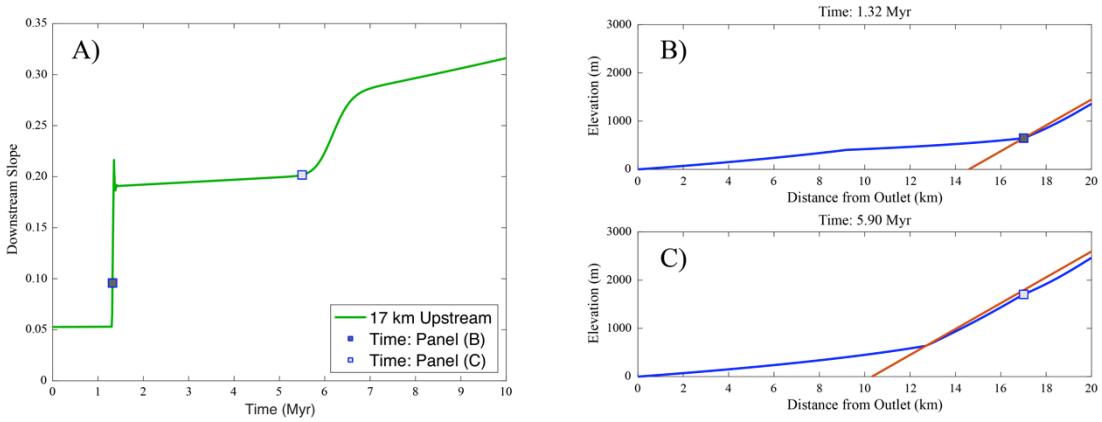

Fig. 27. Evolution of a node's downstream slope (A) and time slices of the stream's evolution demonstrating the influence of the soft over hard positively dipping contact (B) and the uplift knickpoint (C) on the downstream slope of a node. Note the rapid increase in slope as the contact passes the node, the sustained period of very slow slope growth after the contact's passing, the rapid increase in slope as the uplift knickpoint passes, and the moderate rate of slope increase after the uplift knickpoint's passing. This model run involves a contact dipping 15 degrees between a soft unit (K=3.8x10^{-8} m$^{-0.5}$yr^{-1}) overlying a hard unit (K=2x10^{-9} m$^{-0.5}$yr^{-1}) and a change in uplift rate at time 0 in panel (A) from 5x10^{-5} m/yr to 2.5x10^{-4} m/yr. The node examined in panel (A) is located 17 km upstream and

identified by gray squares in panels (B) and (C) at times indicated by corresponding gray squares in panel (A).

upstream position of a higher k_{sn}. Intuitively, the wave produces no change in k_{sn} as it propagates upstream if the entire stream has the same k_{sn} as was responsible for generating the transient contact knickpoint. In this case, the transient contact knickpoint simply increases the profile's elevation as it propagates upstream (Fig. 27).

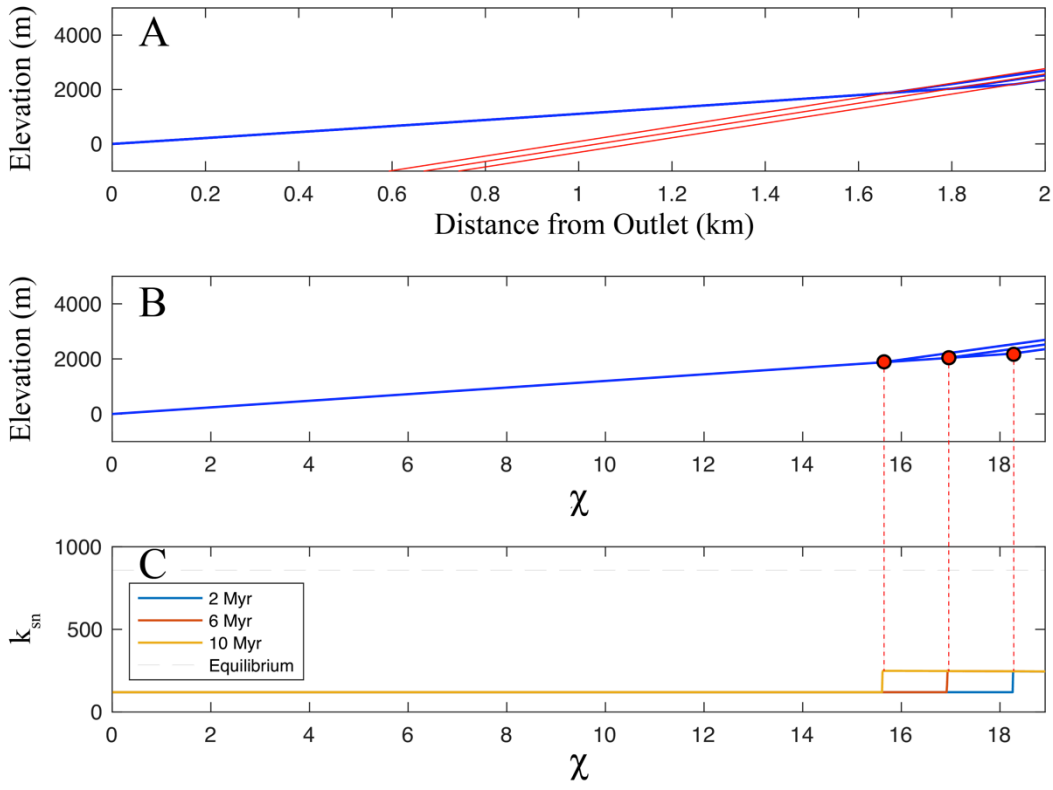

Fig. 27. Model results in real space (panel A), χ-space (panel B), and $\chi - k_{sn}$ space (panel C) for a run with a Hack's coefficient of 12, Hack's exponent equal to 1 (a straight profile), and a soft over hard contact (red line) dipping 15 degrees towards the outlet. The soft unit's K is 3.80×10^{-8} $m^{-0.5}yr^{-1}$, and the hard unit's K is 2×10^{-9} $m^{-0.5}yr^{-1}$. Results are for 2 Myr, 6 Myr and 10 Myr after the contact is first exposed at the stream's head. Uplift rate is constant at 5×10^{-5} m/yr. The red lines in panel (A) and red dots in panel (B) are the contact's positions and outcrop locations at each time step, respectively. Note the rising height of the profile upstream of the contact but spatially and temporally constant k_{sn}.

The fundamental controls on k_{sn} at Position (A) after a transition to the hard unit are 1) the duration of time the contact spends between Positions (A) and (B) (in the short term), 2) the erodibility of the hard unit (assuming the soft unit's K is held constant), and 3) the contact's celerity downstream from Position (B). If the contact's celerity decreases while between Positions (A) and (B), Position (A) will more closely approach its equilibrium downstream slope during its rapid elevation rise while located immediately upstream from the contact. Likewise, if the hard unit's K decreases, Position (A) will experience a greater rise in downstream slope while located immediately upstream from the contact, though the time required to reach steady state steepness also increases as the K_f/K_i ratio moves further from unity (Fig. 26). Since each position's adjustment to the sudden exposure of the hard unit propagates upstream as transient contact knickpoints, Position (A)'s steepness also depends on the magnitudes of transient contact knickpoints that have previously passed. Importantly, planar contacts propagating through a convex profile advance downstream at a spatially variable rate inversely correlated with the acute angle between the contact and stream profile. Therefore, as the contact progresses downstream, its celerity changes, and adjacent positions either adjust marginally closer to or further from steady state while located immediately upstream of the contact (hence the convexity in χ-space in the baseline runs). The resulting transient contact knickpoint waves propagate upstream, marginally adjusting k_{sn} as they advance. The contact's arrival at the outlet establishes a stable boundary condition, allowing the position immediately upstream of the contact to reach topographic steady state. This final wave, or outlet knickpoint, propagates upstream and brings the entire profile to equilibrium.

A hard over soft positively dipping contact behaves similarly to the soft over hard positively dipping contact case. Waves generated at each position still increase in magnitude as contact celerity decreases and the soft unit's K increases, but these waves decrease k_{sn} as they progress upstream (e.g., Fig. 13(A1 and B1)).

5.1.2. Negatively Dipping Contacts with Upstream Celerity

As described in the 2-D modeling study by Forte et al. (2016), the exposure of a soft over hard rock with a horizontal dip induces a transient contact knickpoint to propagate upstream from the contact and reduce the soft unit to a thin veneer draped upon the contact. As contacts dip more steeply towards the basin divide, the soft unit retains more of its relief in the wake of the transient contact knickpoint. Given the simplicity of this study's 1-D modeling, the soft over hard positively dipping contact scenario will now be explored with greater detail using insight from the baseline runs.

Consider a horizontal contact with a soft unit overlying a hard unit. Initially, the stream is of low relief and entirely composed of the soft unit. Now, consider two adjacent positions, where Position (A) is located just upstream from the outlet and Position (B) is located just upstream from Position (A). When the contact migrates upstream past Position (A), Position (A)'s K decreases, and uplift outpaces erosion. Position (A) rises, the downstream slope of Position (B) falls, and uplift now outpaces erosion at Position (B). After Position (B) rises, the next upstream position rises, and the process continues propagating upstream at a rate defined by equation (11). Since the stream's slope in the wake of the transient contact knickpoint cannot reach zero, the contact's rise outpaces the soft unit's rise until only a thin veneer of the soft unit remains. Thus, the transient contact knickpoint communicates a decrease in erosion rates as it propagates upstream, and the

subsequent rise in elevation between the contact and transient contact knickpoint produces the soft unit's low relief (Fig. 29).

The soft unit sustains its low relief because the non-vertical contact migrates upstream and acts as a non-stable local base level for the soft unit. When the contact migrates past a new position along the stream, that position rises and initiates a new incisional wave that propagates upstream and reduces slope. Thus, the soft unit cannot recover its relief, and the constant production and propagation of transient contact knickpoints maintain under-steepened topography throughout the soft unit, where erosion rates fail to keep pace with rock uplift rate. After the very first transient contact knickpoint strips relief by decreasing erosion rates upstream from the contact, subsequent transient contact knickpoints only marginally impact erosion rates and are nearly undetectable as discrete features.

If the contact were to remain in place after passing Position (A), Position (B)'s downstream slope would eventually recover to steady state. If the contact moved slower through the profile, the recovery time for Position (B) would increase, and the frequency with which transient contact knickpoints form would fall. Since k_{sn} throughout the reach upstream from the contact rises when not completely suppressed by transient contact knickpoints and falls upon encountering transient contact knickpoints, slowing the contact's upstream celerity causes the soft unit to retain more of its relief. In other words, the relief of the reach upstream from the contact and downstream from the initial transient contact knickpoint reflects a constant competition between the contact's upstream migration, which acts to lower relief, and the stream's proclivity towards equilibrium, which acts to return to the higher relief steady state that existed prior to the contact's first

exposure. Decreasing contact dip angle increases contact celerity, enhances the rate of elevation rise in the reach between the contact and initial transient contact knickpoint, and produces a more under-steepened reach between the contact and initial transient contact knickpoint. Increasing the soft unit's K increases the celerity of the transient contact knickpoint, lowers the soft unit's steady state relief, and produces a more under-steepened reach between the contact and initial transient contact knickpoint (Fig. 29).

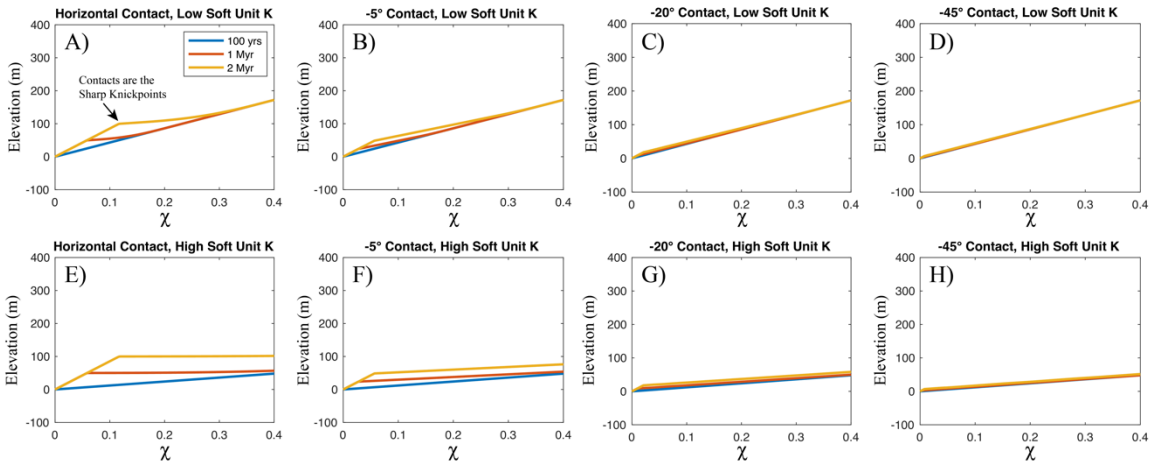

Fig. 29. Influence of contact dips and K on the relief of profiles after the exposure of a contact with varying dip angles. Decreasing contact dip increases contact celerity and drive down relief, while increasing K decreases the initial k_{sn} in the soft unit and increases the upstream celerity of the transient contact knickpoint and rate of adjustment of the profile to the exposure of the contact. Uplift rate is constant at 5×10^{-5} m/yr, the hard unit's K is 2×10^{-9} $m^{-0.5}yr^{-1}$, and the soft unit's K is 5.6×10^{-9} $m^{-0.5}yr^{-1}$ in panels (A-D) and 3.8×10^{-8} $m^{-0.5}yr^{-1}$ in panels (E-H).

k_{sn} at a position upstream of the contact depends upon 1) the contact's celerity spanning from when it passed the first node upstream from the outlet to when the most recent transient contact knickpoint to reach the position was generated, and 2) the soft unit's K, assuming the hard unit's K is held constant. Controls on the contact's celerity include the rock uplift rate and the acute angle between the contact and stream profile as measured upstream of the contact, a function of both unit's K values and the contact dip

angle. The soft unit's K sets the equilibrium k_{sn} for a position and the transient contact knickpoints' celerity, while both units' K values determine the magnitude of transient contact knickpoints (as set by the rate at which a position adjusts its elevation in response to changing erodibility) (Fig. 30), and the profile's steepness between the contact and transient contact knickpoint.

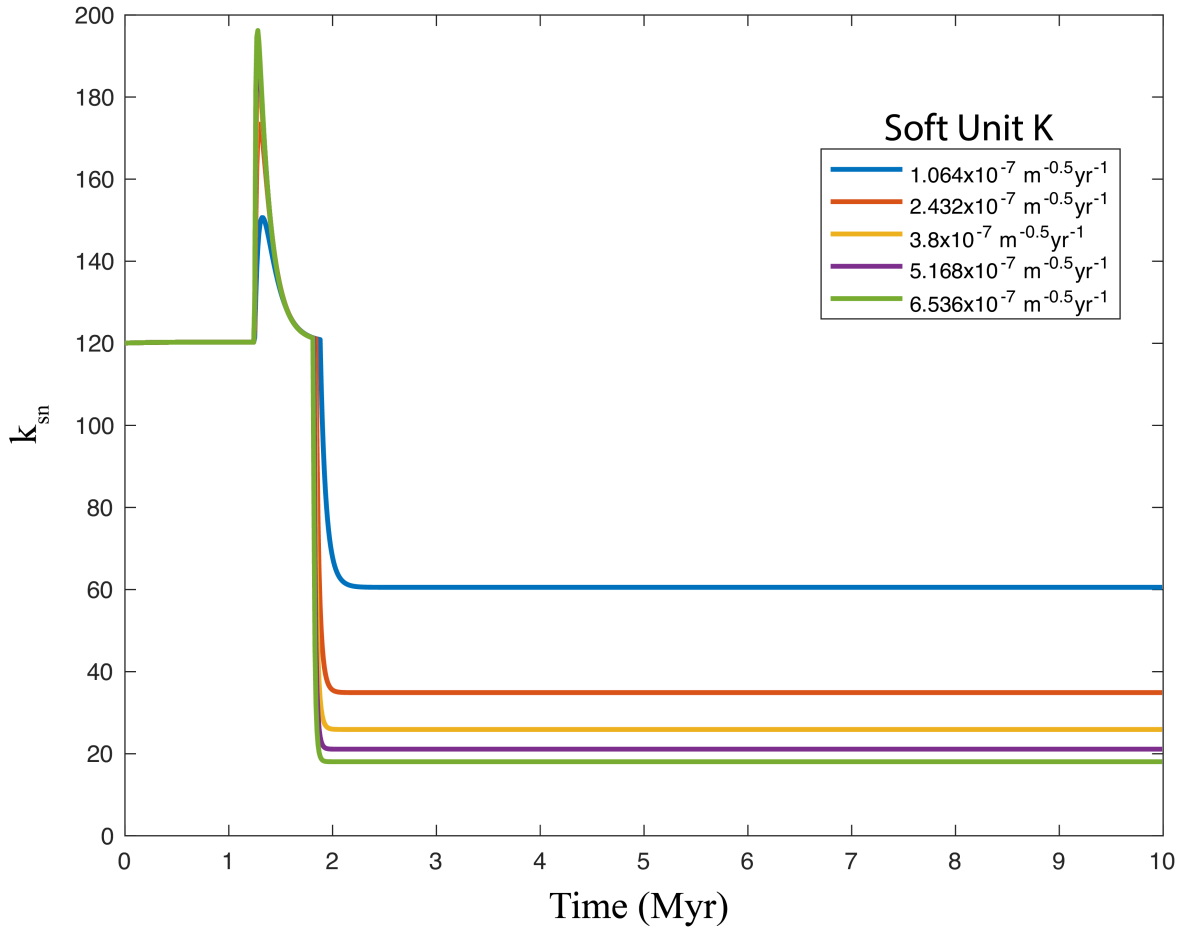

Fig. 30. Adjustments of k_{sn} in response to a change from a hard (K=3.80x10^{-8} m$^{-0.5}$yr^{-1}) unit to a soft unit for varying soft unit K values. All models have a constant uplift rate of 5x10^{-5} m/yr and a -15 degree dipping contact. The k_{sn} data displayed is for a node located 20 m upstream. Note that the rate of adjustment to a higher erodibility increases with the soft unit's K.

The baseline runs suggest that increasing K indeed reduces relief between the contact and initial transient contact knickpoint, though increasing contact celerity emerges

as more efficient at reducing relief (given the parameter space explored). If contacts advance upstream too slowly, or if the K_f/K_i ratio is too low, transient contact knickpoints occur too infrequently or with too little magnitude to establish a significantly under-steepened reach upstream of the contact. Furthermore, the stream's concavity causes a shallow planar contact to decrease celerity as it propagates upstream and a steep planar contact to increase celerity as it propagates upstream. Again, this means k_{sn} evolves upstream of the contact, as transient contact knickpoints continue to propagate. For all of the soft over hard negative contact dip baseline runs, contact dips are sufficiently shallow for the contact's upstream celerity to only decrease through time.

When a hard over soft negatively dipping contact exists, the contact increases K at Position (A) and causes erosion rate to greatly outpace uplift rate. The resulting elevation drop at Position (A) causes Position (B) to over-steepen and fall. This wave translates upstream as a transient contact knickpoint. However, this wave advances with relatively low celerity, since it originates in a hard unit. If the transient contact knickpoint's celerity is sufficiently slow with respect to the contact's celerity, it hardly advances ahead of the contact and produces a steep cliff. In this scenario, when a position increases erosion rate due to the transient contact knickpoint, it rapidly falls to within the soft unit and quickly approaches topographic steady state steepness (Fig. 31).

As the hard units' K or the contact dip increases, the stable contact and transient contact knickpoints move further apart, and the over-steepened reach between the two knickpoints dampens because their elevation difference spreads a longer distance. As observed in the baseline runs, this reach's steepness can greatly alter uplift knickpoint

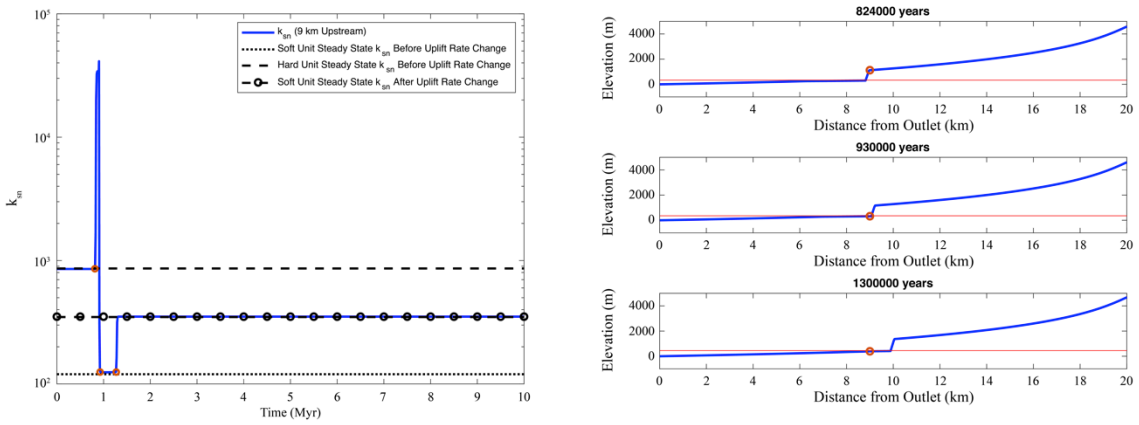

Fig. 31. k_{sn} through time for a position 9 km upstream from the outlet (left panel) and several time slices for the model run (right panels) with the contact in red and position of interest marked by an orange dot. The profile has a hard over soft horizontal contact with a hard unit K equal to $2x10^{-9}$ $m^{-0.5}yr^{-1}$ and soft unit K equal to $3.8x10^{-8}$ $m^{-0.5}yr^{-1}$. The position is first in steady state with respect to the hard unit, becomes oversteepened for a short period of time in the reach between the contact and transient contact knickpoint, approaches topographic steady state in the soft unit prior to encountering the uplift knickpoint, and finally reaches topographic steady state in the soft unit after the uplift knickpoint has passed. The initial uplift rate is $5x10^{-5}$ m/yr and the final uplift rate is $2.5x10^{-4}$ m/yr.

behavior from steady state predictions. Within the over-steepened reach, erosion rates exceed rock uplift rate, and positions act to decrease downstream slope to approach topographic steady state. If the reach upstream from the contact were at topographic steady state, a base level perturbation would raise the elevation of the position just downstream from the contact, decrease downstream slope of the position just upstream from the contact (in the hard unit), and drive the entire hard unit's reach towards a new steady state k_{sn}. However, when the reach upstream from the contact is severely oversteepened, a rise in elevation of the position just downstream from the contact has a negligible effect on the downstream slope of the first position in the over-steepened reach. The first position in the over-steepened reach continues to lower its elevation as if the uplift knickpoint never approached, and the uplift knickpoint fails to propagate past the

contact. As the magnitude of uplift rate change increases, so does the rise in elevation downstream from the over-steepened reach. Therefore, the threshold steepeness required for the over-steepened reach to prevent the passage of the uplift knickpoint increases.

5.2. Implications for Knickpoint Celerity and Vertical Velocity

In line with similar studies (e.g., Forte et al., 2016; Perne et al., 2017; Yanites et al., 2017), this study indicates that non-vertical contacts perturb stream profiles from topographic steady state. Due to a stream's concavity, a planar contact's celerity varies through time, and steepness can evolve for reaches far upstream of a contact. Assuming positively dipping contacts exclusively migrate downstream and negatively dipping contacts exclusively migrate upstream, hard over soft contacts produce over-steepened upstream reaches, while soft over hard contacts produce under-steepened upstream reaches.

When an uplift knickpoint initiates at base level, it first propagates through a reach at topographic steady state. If it propagates past a vertical contact into a new unit at topographic steady state, its vertical velocity does not change because both units share identical uplift rates and slope exponents (Figure 32). On the other hand, knickpoint

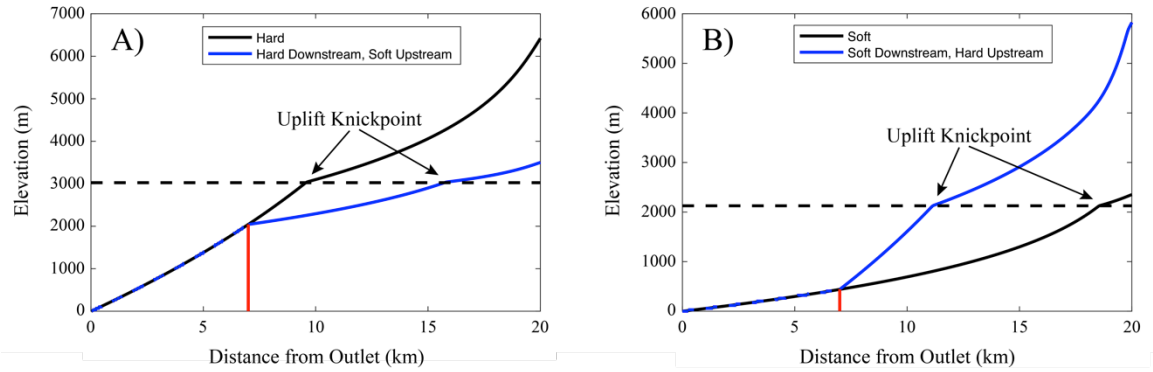

Fig. 32. Model runs 10 Myr (A) and 7 Myr (B) after a change in uplift rate from $5x10^{-5}$ m/yr to $2.5x10^{-4}$ m/yr. Contacts (red lines) are vertical, and uplift knickpoints propagate vertically at equal rates regardless of stratigraphic order or the presence of contacts.

celerity changes according to the erodibility upstream of the contact. However, a non-vertical contact initiates transient contact knickpoints that drive the upstream unit's reach out of topographic equilibrium and causes its k_{sn} to differ from the steady state analytical prediction (equation (5)). Downstream of a transient contact knickpoint, an under-steepened reach (produced by a soft over hard contact) behaves as if its uplift rate has fallen, while an over-steepened reach (produced by a hard over soft contact) behaves as if its uplift rate has risen. Each time the contact passes a new node, the node's rapid elevation adjustment changes the local base level for the upstream reach. Since the contact passes new nodes at a nearly (due to the stream's concavity) constant rate, over time, these discrete perturbations collectively behave as a sustained change in the rate of local base level change for the reach upstream of the contact. As previously discussed, the contact's celerity sets the frequency with which individual nodes transition to a new erodibility, while the K_f/K_i ratio sets the magnitude of elevation change experienced by a node upstream of a contact. Together, these factors set the rate of local base level change felt upstream of a contact. In equation (2), changing the rate of base level change is equivalent to changing the uplift rate. Local base level for the reach upstream of a soft over hard contact rises, effectively decreasing the reach's net uplift rate. On the other hand, local base level for the reach upstream of a hard over soft contact falls, effectively increasing the reach's net uplift rate. This net uplift rate, which accounts for changes in local base level caused by a non-vertical contact's migration is henceforth referred to as the effective uplift rate (U_{eff}). Therefore, an uplift knickpoint transitioning into a reach upstream from a contact not only experiences a change in K but also a change in initial uplift rate from U_1 to U_{eff}.

To test whether a change in uplift knickpoint vertical velocity upstream from a non-vertical contact is driven by a change in U_1, I ran complementary soft over hard scenarios in which $n = 1$ (See Section 7). I also ran cases with $n < 1$, but for this case, the uplift knickpoint widens into an expanding knickzone and becomes difficult to accurately track past the contact (e.g., Royden and Taylor Perron, 2013). The n=1 runs each contain a single contact dipping -5°, and K values were chosen to match the K_f/K_i ratios spanned by the baseline runs while keeping k_{sn} of the hard unit in the complimentary n=1 runs equal to k_{sn} of the hard unit in the baseline runs. When considering equation (10b) as governing knickpoint vertical velocity, the results are consistent with the knickpoint's vertical velocity changing due to a change in initial uplift rate from U_1 to U_{eff}, as the uplift knickpoint does not change vertical velocity upstream from the contact (Fig. 33). Since knickpoint vertical velocity for the case of n=1 solely depends upon U_2, these runs also suggest that a change in U_2 cannot explain the knickpoint's change in vertical velocity when n>1.

Additionally, I tested a change in erodibility upstream from the non-vertical contact as a potential driver for the change in knickpoint vertical velocity by comparing $n = 1$ runs with -5° and vertical contact dips. Under this case, celerity in χ-space solely depends upon K when steady state is maintained (equation (12b)). Results for these simulations show both knickpoints advancing upstream with identical celerities in χ-space, suggesting that transient contact knickpoints do not alter the effective erodibility of upstream units (Fig. 34).

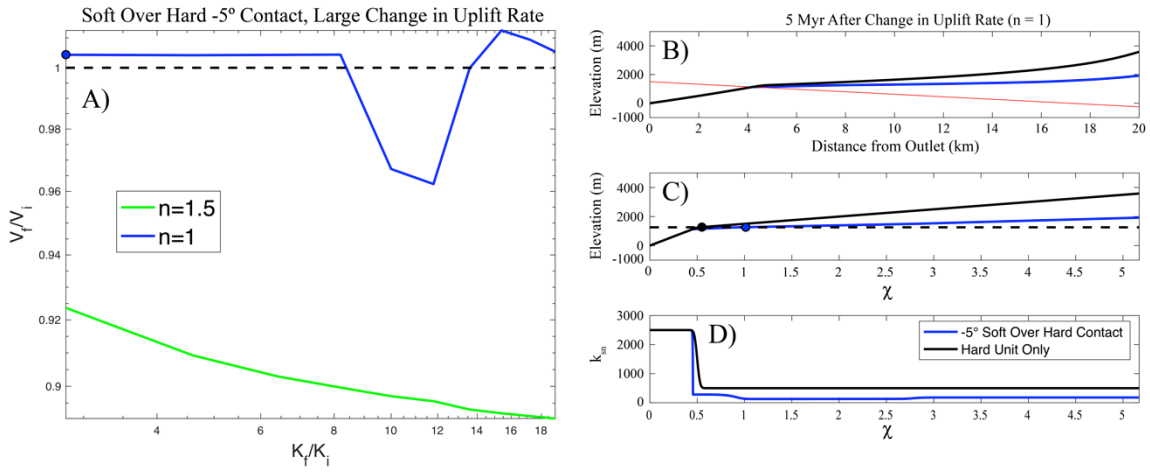

Fig. 33. Panel (A) shows the ratio between uplift knickpoint vertical velocity after and before passing a -5° soft over hard contact. The uplift knickpoints in each run are produced by a change in uplift rate from $5\text{x}10^{-5}$ m/yr to $2.5\text{x}10^{-4}$ m/yr. Panels (B-D) show a run marked by the blue dot in Panel (A) in which the hard unit's K=$1\text{x}10^{-7}$ yr^{-1} and the soft unit's K=$2.8\text{x}10^{-7}$ yr^{-1}. Uplift knickpoints in panel (B) are indicated by black and blue dots. Note that the change in velocity in panel (A) is likely within the numerical scheme and data extraction method's error for knickpoint vertical velocity when n=1.

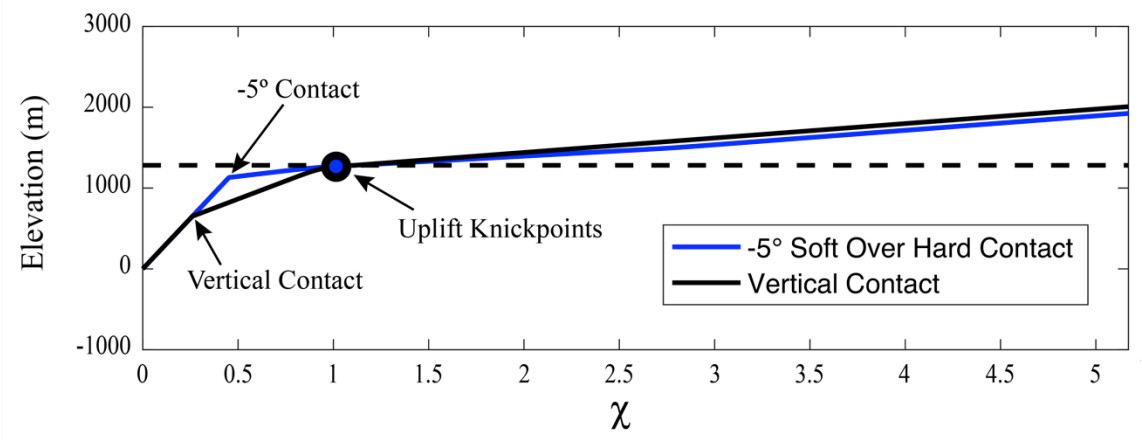

Fig. 34. Comparison of runs with vertical and -5° contact dips with a hard unit (K=$1\text{x}10^{-7}$ yr^{-1}) exposed downstream from a soft unit (K=$2.8\text{x}10^{-7}$ yr^{-1}) and n equal to 1. The vertical contact outcrops at the same distance upstream that the uplift knickpoint crosses the -5° contact so that the uplift knickpoint transitions to the soft unit at the same location in both runs. Note that both uplift knickpoints (large black and smaller blue dots) propagate with identical celerities and vertical velocities upstream from the contact.

These tests suggest that the change in vertical velocity of uplift knickpoints observed in the baseline runs can be attributed to a change in U_1 upstream of a contact to U_{eff}. Under this assumption, the following statements can be made:

1. The effective uplift rate (U_{eff}) and slope exponent determine the sign of the change in celerity and vertical velocity of uplift knickpoints after propagating through a discrete change in K, such that the sign of the quantity $(n-1)(U_{eff}-U_1)$ determines whether the uplift knickpoint increases (quantity > 0), decreases (quantity < 0), or does not change (quantity = 0) its vertical velocity and celerity (Fig. 35).
2. For $n \neq 1$ scenarios, when holding K_i and U_1 constant, K_f and contact celerity (controlled by contact dip angle, U_2, and the stream's initial profile shape) control the magnitude of change in celerity and vertical velocity of uplift knickpoints after propagating through a discrete change in K. The change in uplift knickpoint celerity and vertical velocity scale with the contact's celerity and as the K_f/K_i ratio deviates from 1 (Fig. 35). Since a planar contact's celerity with respect to a concave stream profile changes very slowly throughout individual runs, so do vertical velocities and celerities of uplift knickpoints upstream of non-vertical contacts when $n \neq 1$. While this presents itself as slightly sub-unity R^2 values for some knickpoint vertical velocities calculated with linear regressions, in my simulations, the gradual change in contact celerity within individual runs plays an extremely small role relative to contact dip, U_2, and the K_f/K_i ratio in setting knickpoint vertical velocity and celerity upstream from a non-vertical contact.

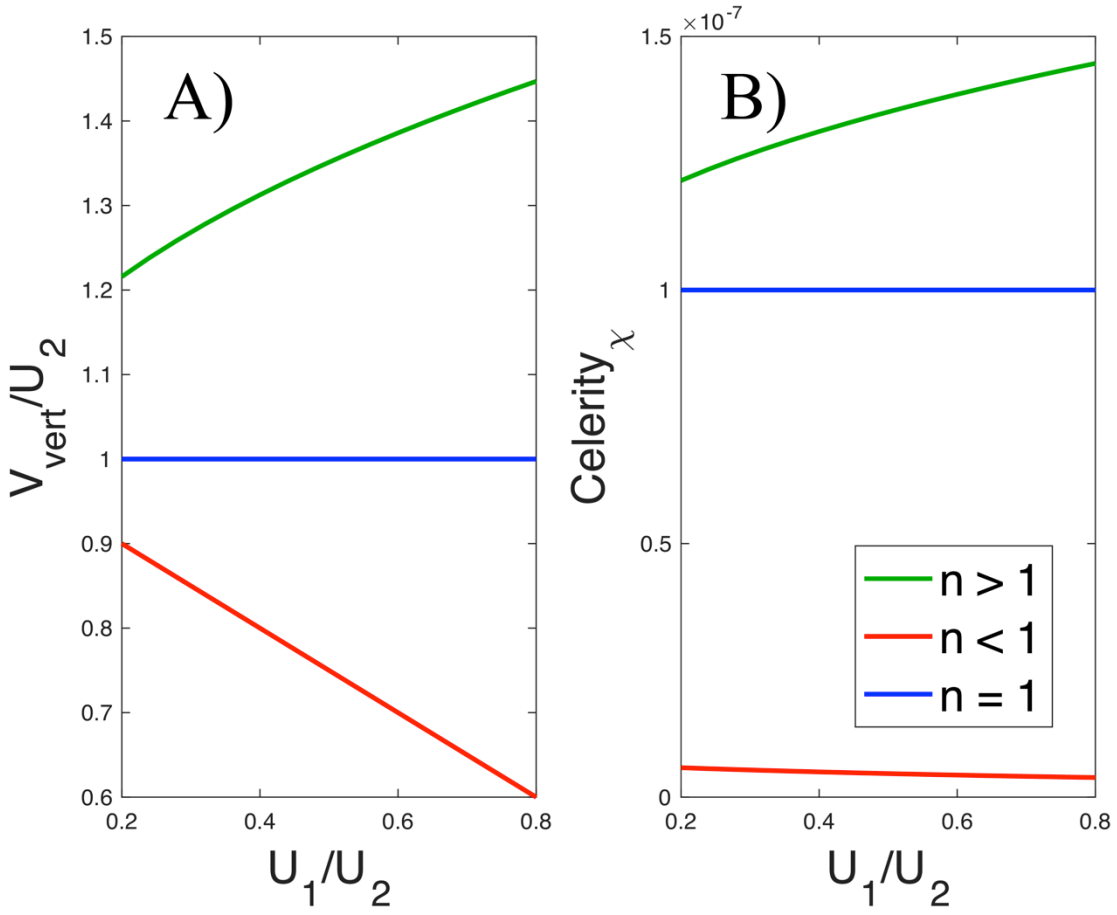

Fig. 35. Uplift knickpoint vertical velocity normalized by final uplift rate (Panel (A)) and celerity in χ-space (Panel (B)) as functions of the initial and final uplift rates. U_1 ranges from 5x10^{-5} m/yr to 2x10^{-4} m/yr, and U_2 = 2.5x10^{-4} m/yr (Panel (A)). n=1.5 and 0.67 for the cases of $n > 1$ and $n < 1$, respectively. K=2x10^{-9} m$^{-0.5}$yr^{-1}, 1x10^{-7} yr^{-1}, and 1.32x10^{-6} m$^{0.33}$yr^{-1} for the cases of $n > 1$, $n = 1$, and $n < 1$, respectively. To find the influence of a contact on vertical velocity and celerity, change U_1 to U_{eff}.

5.3. Implications for Knickpoint Prominence

Equation (14) dictates that a knickpoint's prominence changes with erodibility, even if a contact is vertical and topographic steady state is maintained. However, since the reach upstream of a non-vertical contact has a steepness set by U_{eff} rather than U_1, prominence no longer follows the analytical prediction. Estimating U_{eff} as greater than U_1 for a hard over soft contact and less than U_1 for a soft over hard contact (by magnitudes set by the

contact's celerity and K_f/K_i ratio) qualitatively accounts for the deviations between observed and predicted uplift knickpoint prominences in the baseline runs.

The case of a soft over hard positively dipping contact presents a particularly complex relationship (including a kink) between knickpoint prominence, uplift rate, the K_f/K_i ratio, and contact dip. If assuming topographic steady state, decreasing the hard unit's K causes a non-linear increase in the uplift knickpoint's prominence. However, with a non-vertical contact, decreasing the hard unit's K, increasing the rock uplift rate, and lowering a contact's dip all decrease U_{eff} in the upstream hard unit. Therefore, the kink is an inflection point at which the decreased U_{eff} caused by the increased elevation of nodes upstream of the contact outperforms the decreased erodibility upstream of the contact. The inflection point's location shifts to lower K_f/K_i ratios as the contact steepens and the change in rock uplift rate decreases because both of these conditions cause contact celerity to decrease and U_{eff} to increase towards the rock uplift rate. To counteract the influence of a steepened contact dip and lowered rock uplift rate on U_{eff}, the hard unit's K must decrease. While inflection points only form in the soft over hard positive dip directions (Fig. 10), the competition between the stream's proclivity towards steady state steepness upstream of a contact and the impact of a sudden change in K on U_{eff} is expressed in the hard over soft positive contact dip scenarios as the 'fanning out' of prominence curves as the K_f/K_i ratio moves further from unity (Fig. 15).

For negative contact dip scenarios, changing the K_f/K_i ratio further from unity does not compete with, but rather amplifies, the steady state prediction of changing K on knickpoint prominence. For example, with a hard over soft stratigraphy and negatively dipping contact, lowering the hard unit's K increases a node's drop in elevation after

changing erodibility. This further increases U_{eff} of the reach upstream of the contact and causes an uplift knickpoint's prominence to surpass the steady state prediction in the hard unit (Fig. 24).

5.4. Multi-Contact Runs

I conducted additional runs to explore the influence of multiple contacts on uplift knickpoints. To test the abruptness of a transition to a new erodibility on the propagation of uplift knickpoints, I compared a run with a soft over hard negatively dipping contact to a run with an identical upstream change in K accomplished over four contacts forming five progressively softer 150 m thick units (Fig. 36). The location of the upstream-most contact in the four contact run matches the location of the contact in the single contact run. Prior to the change in uplift rate, the exposure of progressively harder units initiates transient contact knickpoints that propagate past contacts into further upstream units and decrease relief in their wakes. These waves become extremely subtle, even in $\chi - k_{sn}$ space, after passing a contact, and they merge with the uplift knickpoint when the two waves collide. Between both runs, the uplift knickpoint has nearly identical prominences in the softest unit. In the four contact scenario, k_{sn} both upstream and downstream from the uplift knickpoint in the softest unit slightly exceeds that for the single contact run. This suggests that, so long as uplift knickpoints can propagate past contacts, their prominence in a new unit only weakly depends upon the stream reach's length across which a change in K occurs. It should be emphasized that this does not hold for scenarios in which the uplift knickpoint fails to propagate past a contact, which occurs in baseline runs with hard over soft horizontal contacts and sufficiently low K hard units.

After propagating into the softest unit, deviations in uplift knickpoint elevations and, more notably, distances from the outlet between the two runs result from the uplift knickpoint crossing the downstream-most contact in the four contact run earlier than it crosses the contact in the single contact run (Fig. 36). Once the knickpoint crosses a contact, it enters an under-steepened reach in which vertical velocity decreases and celerity increases. As a very fine detail, since the four contact scenario leaves the upstream soft unit reach slightly less under-steepened than the single contact scenario, the uplift knickpoint's vertical velocity in the soft unit is slightly greater in the four contact scenario than in the single contact scenario.

When a change in uplift rate perturbs river profiles with alternating hard and soft subhorizontal layers with negatively dipping contacts, the uplift knickpoints follow the general trend illuminated by the baseline runs and increase vertical velocity in hard over-steepened units while decreasing vertical velocity in soft under-steepened units (Fig. 37A-B). Celerity also increases in the soft units and decreases in the hard units. Interestingly, transient contact knickpoints generated in soft units branch into two distinct waves upon interacting with an upstream hard unit and fail to propagate into the next soft unit. On the other hand, transient contact knickpoints generated in hard units continue to propagate upstream and often remain detectable after passing through several contacts. With horizontal contacts, the uplift knickpoint fails to propagate past the first contact it encounters, regardless of the upstream unit's erodibility. Under this scenario, the knickpoint merges with the contact and adopts the contact's vertical velocity (Fig. 37C).

As an uplift knickpoint propagates into a hard unit with subhorizontal negative contacts, the hard unit becomes a near-shear cliff with k_{sn} far exceeding steady state, and

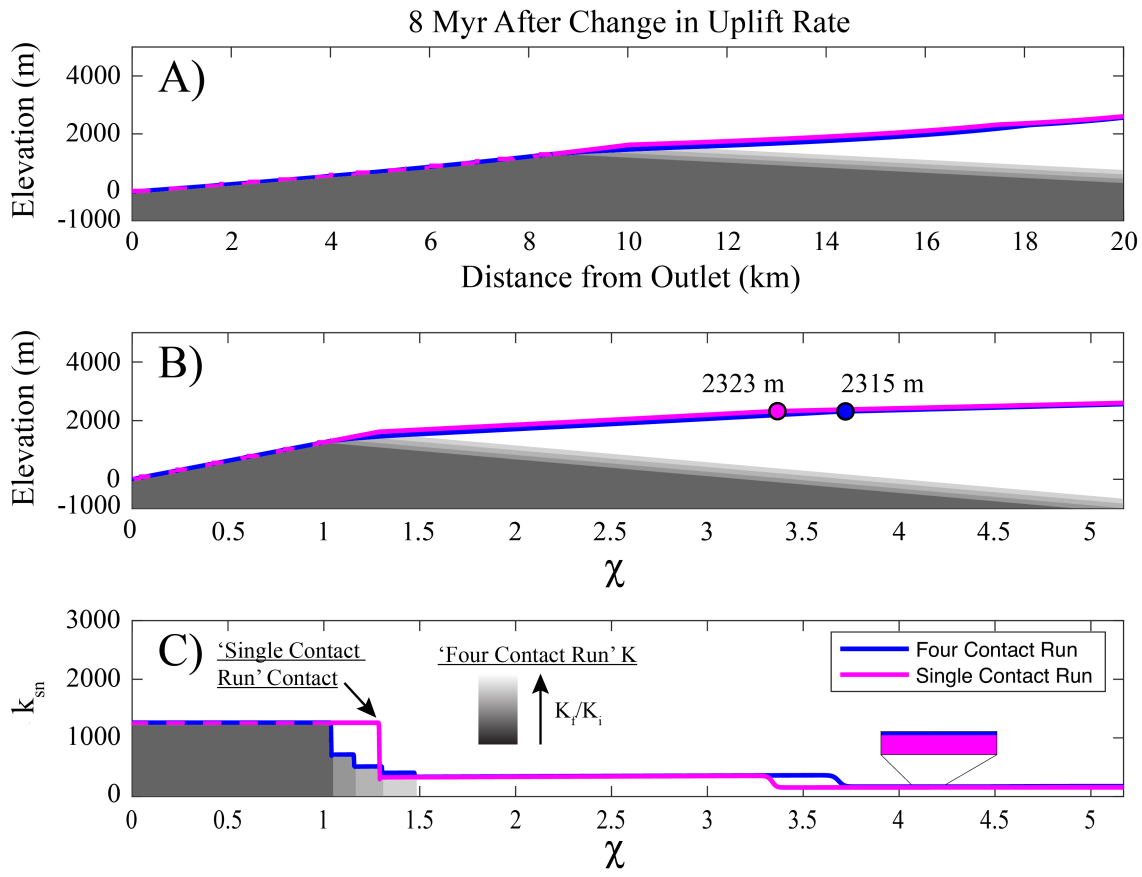

Fig. 36. Comparison of soft over hard runs with identical initial and final K values but different numbers of -5° dipping contacts 8 Myr after a change in uplift rate from $5x10^{-5}$ m/yr to $2.5x10^{-4}$ m/yr. n is equal to 1.5. The blue profile has four contacts that form 5 progressively softer units, and the magenta profile experiences the same change in K with a single contact. The magenta profile's contact is located at the same elevations as the upstream-most contact on the blue profile. Contacts are in red in panel (A), and uplift knickpoints are indicated by colored circles in panel (B).

the uplift knickpoint becomes nearly indistinguishable. Further downstream, as new contacts outcrop, individual units continue to steepen and flatten as transient contact knickpoints continue propagating upstream. Because transient contact knickpoints also continue to propagate upstream ahead of the uplift knickpoint, k_{sn} in each unit upstream from the uplift knickpoint varies through time. Therefore, when an uplift knickpoint propagates into a given unit, its prominence, vertical velocity, and celerity partially depend upon the nature of transient contact knickpoints that previously propagated through the

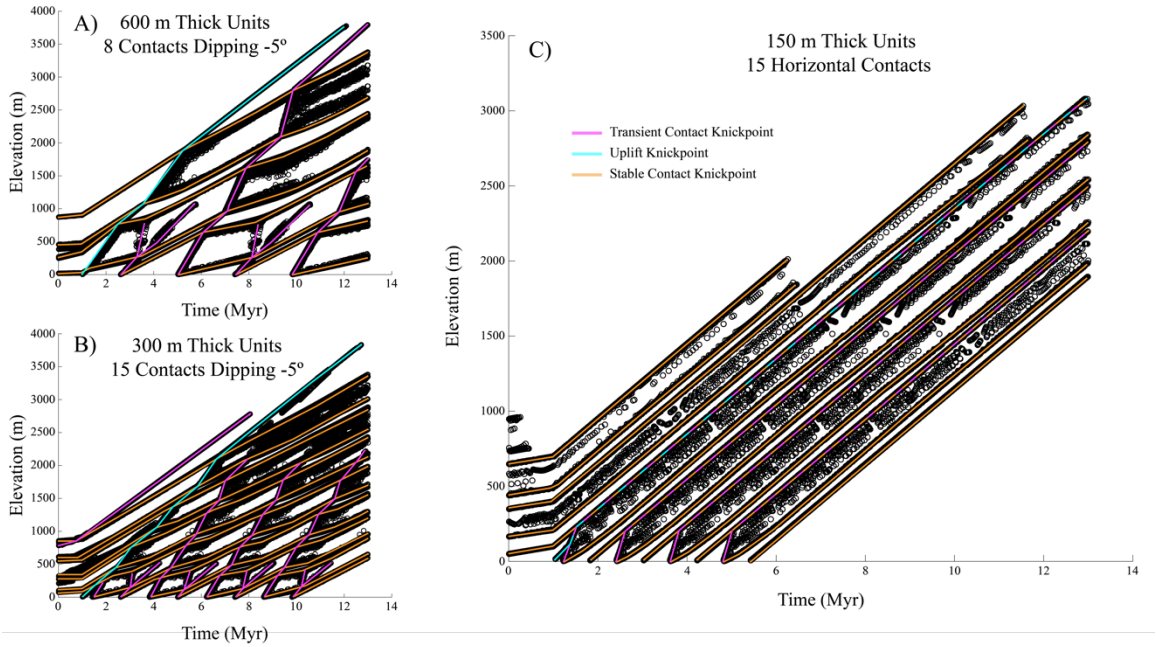

Fig. 37. Time elevation plots for various runs with layered hard (K=2x10^{-9} m$^{-0.5}$yr^{-1}) and soft (K=2x10^{-8} m$^{-0.5}$yr^{-1}) stratigraphy. Note that the uplift knickpoint and transient contact knickpoints fail to propagate past horizontal contacts and change vertical velocity after propagating past subhorizontal contacts.

unit. Based on the multi-contact runs with negative dips, the general trends found in the baseline runs hold, and soft units under-steepen, while hard units over-steepen. However, since the degree of under-steepening or over-steepening does not follow a monotonic trend with successive upstream hard and soft units, the prominence of an uplift knickpoint also does not follow a monotonic trend in each unit (Fig. 38). In other words, the uplift knickpoint's prominence exceeds steady state predictions in hard units and remains below steady state predictions in soft units, but prominence can fluctuate with each successive hard or soft unit because transient contact knickpoints operate on the stream while the uplift knickpoint propagates.

For the case of alternating hard and soft layers with shallow positive dips, easily detectable transient contact knickpoints do not exist throughout the profile. As the uplift knickpoint propagates through the profile, its prominence follows the findings from the

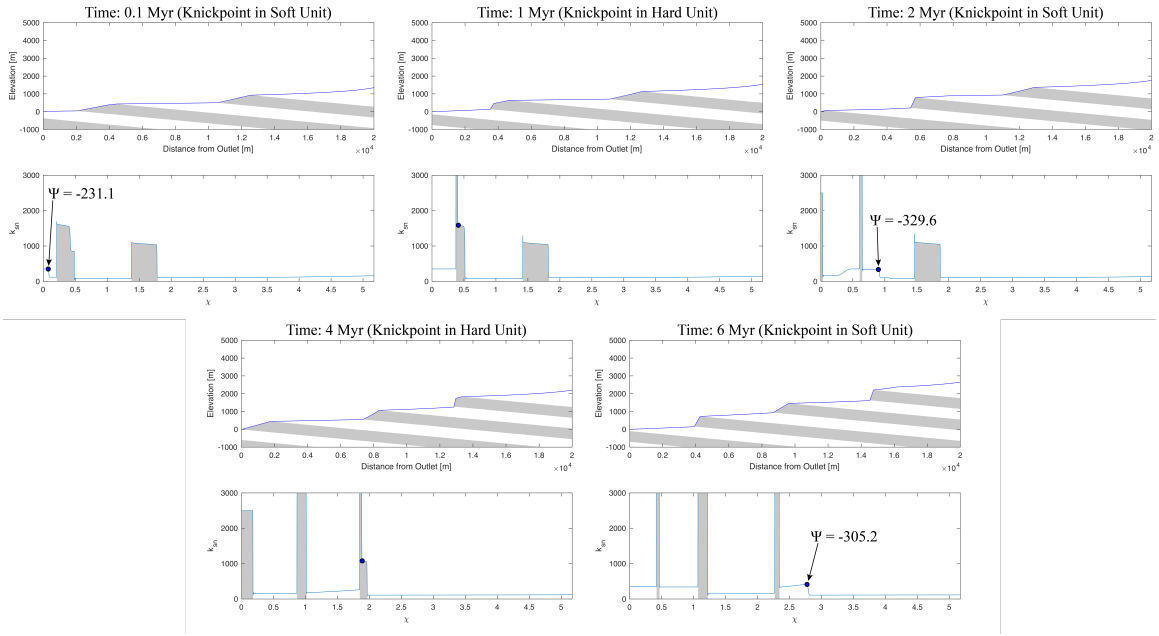

Fig. 38. Uplift knickpoint (blue dot) propagating through layered hard (grey, K=2x10^{-9} m$^{-0.5}$yr^{-1}) and soft (white, K=2x10^{-8} m$^{-0.5}$yr^{-1}) stratigraphy with negative contact dips. Time is after a change in uplift rate from 5x10^{-5} m/yr to 2.5x10^{-4} m/yr.

baseline runs, as soft over-steepened reaches have prominences exceeding their predicted steady state values and hard under-steepened reaches have prominences less than their predicted steady state values. Since transient contact knickpoints do not significantly alter steepness (as is the case with negatively dipping contacts), prominences in each successive hard or soft unit follow monotonic trends, where the uplift knickpoint becomes progressively less prominent in successive hard units and progressively more prominent in successive soft units (Fig. 39). The steepness of each successive upstream hard and soft unit prior to the arrival of the uplift knickpoint also progressively converge towards one another, albeit very gradually. The uplift knickpoint's rapid propagation through each hard unit complicates accurately measuring its vertical velocity in these units, though visual inspections of model runs suggest uplift knickpoints propagate at greater vertical velocities in the hard units than in the soft units.

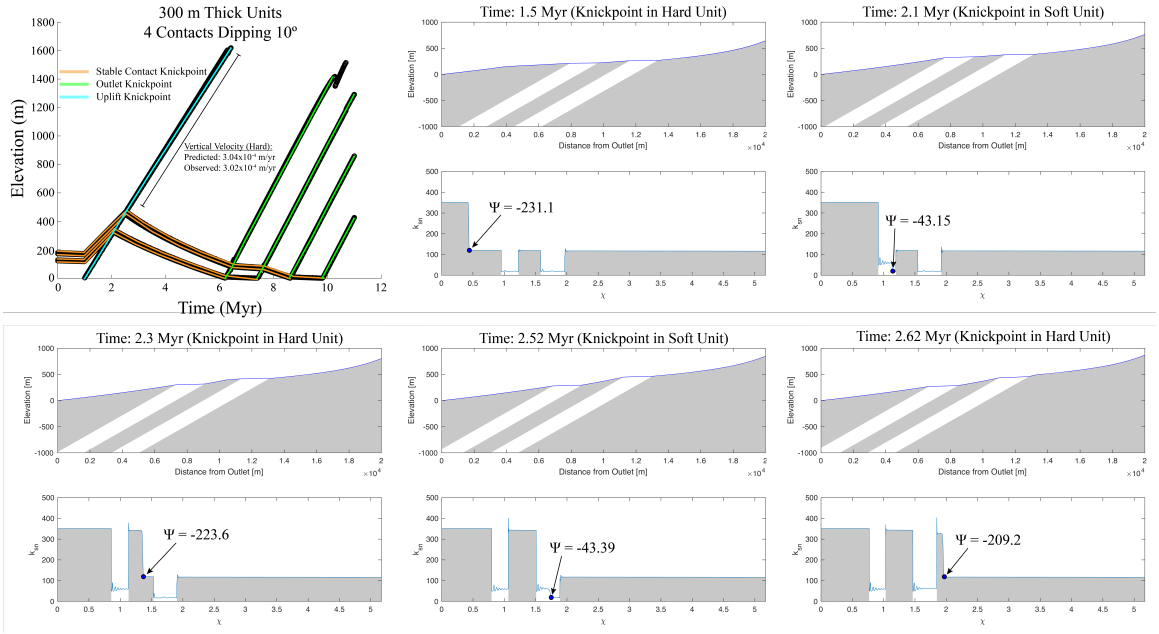

Fig. 39. Uplift knickpoint (blue dot) propagating through layered hard (grey, K=3.8x10^{-8} m$^{-0.5}$yr^{-1}) and soft (white, K=7.22x10^{-7} m$^{-0.5}$yr^{-1}) stratigraphy with positive contact dips. A change in uplift rate from 5x10^{-5} m/yr to 2.5x10^{-4} m/yr occurs at 1 Myr, and the times on each time slice correlate with the x-axis of the time-elevation plot in the upper left.

The multi-contact runs support the behavior observed in the baseline runs and highlight the importance of secondary subtler waves of incision (i.e., transient contact and outlet knickpoints) in determining the change in vertical velocity and prominence of uplift knickpoints by setting the degree to which each position along the profile is either under- or over-steepened. Since they include relatively powerful transient contact knickpoints that significantly alter the profile's steepness, runs with negatively dipping contacts are more difficult to predict knickpoint behavior in than runs with positively dipping contacts.

5.5. Implications for Natural Settings

While this study's 1-D model lacks hillslope diffusion and basin divide migration processes, it offers a level of simplicity enabling for a clear description of the role of discrete changes in erodibility on profiles governed by the SPIM. I emphasize that, while at times enhanced for greater model sophistication (e.g., Lague et al., 2005), the simple

version of the SPIM used in this study is often cited as a basis for tectonic interpretation, and similar 1-D studies are routinely conducted to explore the fundamental effects of specific perturbations on stream profile evolution (e.g., Beeson and McCoy, 2020). Specifically, I find the critical roles of contact celerity and the K_f/K_i ratio in determining the degree to which a contact perturbs upstream reaches from equilibrium. Fast contact celerity (most often resulting from near horizontal contact dips and high uplift rates) and large contrasts in erodibility cause the greatest deviations from steady state predictions. Additionally, interactions with transient contact knickpoints formed by hard over soft negatively dipping contacts and incisional waves formed by the exposure of positively dipping contacts at the stream's outlet can further alter the behavior of uplift knickpoints. These secondary waves of incision can also propagate past contacts and make predicting the vertical velocity, celerity, and prominence of uplift knickpoints throughout the profile extremely difficult, even with erodibility constrained.

Though at times the model runs produce physically unrealistic landscapes (e.g., the km-scale shear cliffs formed by horizontal hard over soft contacts), the essence of this study's findings translates to continuous natural settings. Just as in the model space, natural settings do not adjust instantaneously to changes in erodibility. When contacts dip towards the outlet, the new unit's progressive downstream exposure stunts the slope adjustments of reaches upstream of the contact, and stream power throughout the upstream reach cannot drive incision rates to match uplift rates. Rather than the stunting event occurring each time the contact passes a new model node, this process may occur when a contact reaches some critical distance from a location of interest, such that the elevation at this critical distance influences erosion rates at the location of interest. When

contacts dip towards the divide, the contact's celerity causes reaches near the contact to protrude and preferentially erode (Perne et al., 2017). This initiates transient contact knickpoints that sustain over-steepened (hard over soft) or under-steepened (soft over hard) reaches upstream of the contact. Though these transient contact incision waves may not occur as regularly in natural settings as in the model domain, their suspected existence in natural settings is supported by reasonable physical assumptions (Perne et al., 2017), and they exert a clear and meaningful influence on stream profile evolution when assuming this study's simplified erosion model.

My findings apply to many regions commonly investigated with topographic analyses, and in particular, incised plateaus, continental margins, and forearc basins. Each of these landscapes often contain sequences of shallowly dipping layers with moderately contrasting erodibility (e.g., uplifted sedimentary sequences) and/or tilted units of highly contrasting erodibility (e.g., tilted sedimentary sequences juxtaposed with volcanic flows, outcropping intrusions, and exhumed basement), both of which contribute towards creating the necessary conditions for uplift knickpoints to deviate from topographic steady state predictions. If contact celerity is too slow or the K_f/K_i ratio too near unity, U_{eff} may not differ sufficiently from U_1 for knickpoints to deviate from steady state behavior beyond that which may be associated with typical error from the knickpoint extraction process. On the other hand, sufficiently shallow contacts with large contrasts in erodibility may not only drive uplift knickpoint behavior from steady state predictions, but because transient contact knickpoints perturb upstream reaches, projected stream profiles may also yield inaccurate incision depths (Fig. 40). The threshold dip angle for steady state assumptions

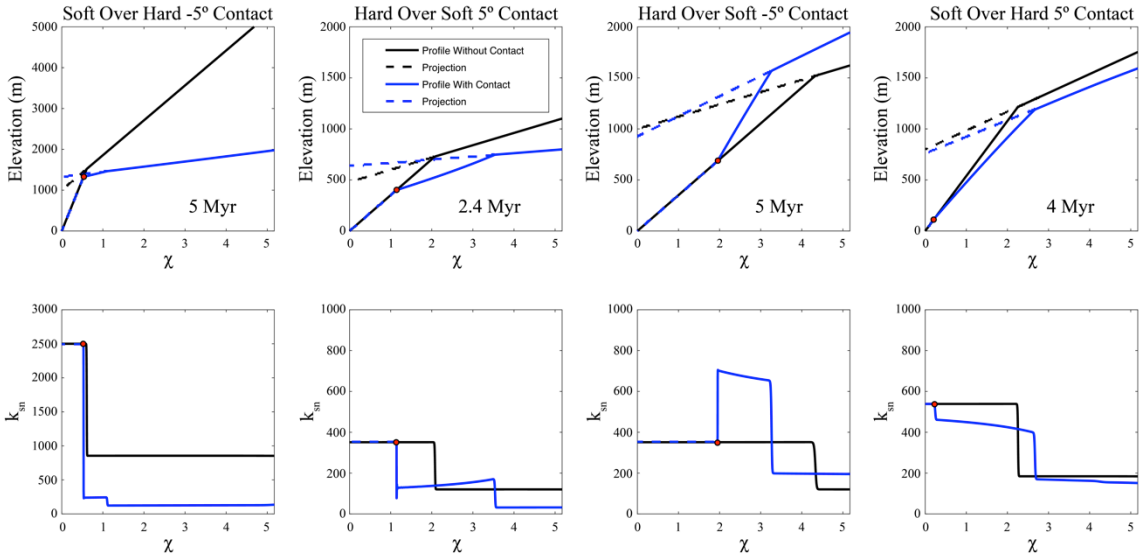

Fig. 40. Profiles (with projections to outlets) in χ-space and $\chi - k_{sn}$ space for selected baseline runs with 5° and -5° contacts and varying stratigraphy. The black profiles lack contacts and share the same K as the unit downstream from the contact on the accompanying blue profiles. The red dots are contact outcrops. Time is with respect to a change in base level that initiated the uplift knickpoint. For all runs, $n = 1.5$.

to remain applicable towards topographic analyses depends upon the relative erodibilities of rock units, rock uplift rate, and stream length, as knickpoint elevations will diverge over time if they propagate through differing stratigraphy. I do not aim to constrain this threshold contact dip angle, and I emphasize that more complex and realistic erosion models incorporating greater dimensions, erosion thresholds, and sediment transport (e.g., Gasparini et al., 2007; Sklar and Dietrich, 2001) may yield more realistic conclusions. Furthermore, while planar contacts serve as a useful simplification towards identifying contact celerity as a critical component to the degree to which contacts perturb upstream reaches, bedrock streams in mountainous terrains often traverse folded units. If rock units fold and contact dips vary, the celerity of contacts along a profile and the magnitude of transient contact knickpoints produced by these contacts will also vary. The spatial and temporal variability of uplift knickpoint behavior will simply reflect the history of each

contact's celerity and change in erodibility conveyed by each contact. Thus, in a hypothetical landscape with highly folded rock and many non-vertical contacts, it is easy to see how accurate topographic analysis may prove extremely difficult (e.g., Yanites et al., 2017), especially without constraining SPIM parameters.

Further complicating topographic analysis, the secondary waves associated with influencing uplift knickpoint behavior (i.e., the transient contact and outlet knickpoints) are quite subtle in the model runs and may not clearly appear in DEM-derived stream profiles, meaning a stream in transience may lack a clear morphological indicator. This is, however, merely hypothesized, as transient contact knickpoints are yet to be identified as such in natural landscapes.

Lastly, since transient contact knickpoints migrate upstream ahead of contacts, uplift knickpoints are only influenced by contacts if they surpass them while propagating upstream. Therefore, for a given change in uplift rate, basin geometry, negative contact dip angle, and K_f/K_i ratio, there exists a maximum distance from the stream's outlet a contact can reside at the onset of change in rock uplift rate for the uplift knickpoint to catch the contact. Of course, this problem further complicates as units fold.

6. Conclusion

The complex patterns of erosion rates observed in previous modeling studies of detachment-limited erosion with layered stratigraphy (Forte et al., 2016; Perne et al., 2017; Yanites et al., 2017) ultimately influence the behavior of upstream propagating knickpoints generated by changes in uplift rate. Using assumptions of knickpoint behavior in steady state topography, I isolated the driver of deviations in knickpoint behavior from steady state to a change in the initial uplift rate of reaches upstream from contacts. This occurs because contacts act as non-stable base levels for upstream reaches and exert a rate of base level change that influences a reach's uplift rate. When all stream power incision model parameters are known, knickpoints deviate from steady state assumptions in predictable ways. However, secondary incisional waves caused by migrating contacts further complicate the behavior of base level perturbations at a given place and time. The vertical velocity, celerity, prominence, and incision depths of knickpoints deviate most from steady state predictions as contact celerity and the cross-contact change in K increases. This modeling work suggests that deviations from steady state assumptions caused by contacts with low along-stream celerity are relatively minor and may account for small differences in knickpoint elevations throughout a landscape with uniform forcings. However, non-vertical contacts, especially those with dips near a stream's slope and between units differing significantly in erodibility, certainly add a layer of complexity to topographic analysis and highlight that landscapes are non-unique solutions that require constraining parameters of transport laws to accurately interpret. There is significant room for additional work in addressing the roles of non-vertical contacts in landscape evolution, and

more sophisticated modeling coupled with field data may help determine the degree to which the processes outlined in this study actually influence natural landscapes.

7. Data Availability

The 1-D bedrock stream evolution and knickpoint data extraction functions are accessible online along with descriptions of simulations and data used in this study (https://zenodo.org/record/3865097#.XtDzOJ5KgdU).

References

Adams, B.A., Whipple, K.X., Hodges, K.V., Heimsath, A.M., 2016. In situ development of high-elevation, low-relief landscapes via duplex deformation in the Eastern Himalayan hinterland, Bhutan: Landscape Response to Hinterland Duplex. J. Geophys. Res. Earth Surf. 121, 294–319. https://doi.org/10.1002/2015JF003508.

Beeson, H.W., McCoy, S.W., 2020. Geomorphic signatures of the transient fluvial response to tilting. Earth Surf. Dyn. 8, 123–159. https://doi.org/10.5194/esurf-8-123-2020.

Bernard, T., Sinclair, H.D., Gailleton, B., Mudd, S.M., Ford, M., 2019. Lithological control on the post-orogenic topography and erosion history of the Pyrenees. Earth Planet. Sci. Lett. 518, 53–66. https://doi.org/10.1016/j.epsl.2019.04.034.

Boulton, S.J., 2020. Geomorphic Response to Differential Uplift: River Long Profiles and Knickpoints From Guadalcanal and Makira (Solomon Islands). Front. Earth Sci. 8, 10. https://doi.org/10.3389/feart.2020.00010.

Campforts, B., Govers, G., 2015. Keeping the edge: A numerical method that avoids knickpoint smearing when solving the stream power law. J. Geophys. Res. Earth Surf. 120, 1189–1205. https://doi.org/10.1002/2014JF003376.

Cook, K.L., Whipple, K.X., Heimsath, A.M., Hanks, T.C., 2009. Rapid incision of the Colorado River in Glen Canyon - insights from channel profiles, local incision rates, and modeling of lithologic controls. Earth Surf. Process. Landf. https://doi.org/10.1002/esp.1790.

Cyr, A.J., Granger, D.E., Olivetti, V., Molin, P., 2010. Quantifying rock uplift rates using channel steepness and cosmogenic nuclide–determined erosion rates: Examples from northern and southern Italy. Lithosphere 2, 188–198. https://doi.org/10.1130/L96.1.

Czarnota, K., Roberts, G.G., White, N.J., Fishwick, S., 2014. Spatial and temporal patterns of Australian dynamic topography from River Profile Modeling. J. Geophys. Res. Solid Earth 119, 1384–1424. https://doi.org/10.1002/2013JB010436.

DiBiase, R.A., Whipple, K.X., 2011. The influence of erosion thresholds and runoff variability on the relationships among topography, climate, and erosion rate. J. Geophys. Res. 116, F04036. https://doi.org/10.1029/2011JF002095.

DiBiase, R.A., Whipple, K.X., Heimsath, A.M., Ouimet, W.B., 2010. Landscape form and millennial erosion rates in the San Gabriel Mountains, CA. Earth Planet. Sci. Lett. 289, 134–144. https://doi.org/10.1016/j.epsl.2009.10.036.

Finnegan, N.J., Roe, G., Montgomery, D.R., Hallet, B., 2005. Controls on the channel width of rivers: Implications for modeling fluvial incision of bedrock. Geology 33, 229. https://doi.org/10.1130/G21171.1.

Flint, J.J., 1974. Stream gradient as a function of order, magnitude, and discharge. Water Resour. Res. 10, 969–973. https://doi.org/10.1029/WR010i005p00969.

Forte, A.M., Yanites, B.J., Whipple, K.X., 2016. Complexities of landscape evolution during incision through layered stratigraphy with contrasts in rock strength. Earth Surf. Process. Landf. 41, 1736–1757. https://doi.org/10.1002/esp.3947.

Foster, M.A., Kelsey, H.M., 2012. Knickpoint and knickzone formation and propagation, South Fork Eel River, northern California. Geosphere 8, 403–416. https://doi.org/10.1130/GES00700.1.

Gasparini, N.M., Whipple, K.X., Bras, R.L., 2007. Predictions of steady state and transient landscape morphology using sediment-flux-dependent river incision models. J. Geophys. Res. 112, F03S09. https://doi.org/10.1029/2006JF000567.

Giachetta, E., Refice, A., Capolongo, D., Gasparini, N.M., Pazzaglia, F.J., 2014. Orogen-scale drainage network evolution and response to erodibility changes: insights from numerical experiments. Earth Surf. Process. Landf. 39, 1259–1268. https://doi.org/10.1002/esp.3579.

Hack, J., 1957. Hack, J.: Studies of longitudinal stream profiles in Virginia and Maryland, in: USGS Numbered Series 294-B, United States Geological Survey, Washington, D.C., 1957. USGS Numbered Ser. 294-B.

Harel, M.-A., Mudd, S.M., Attal, M., 2016. Global analysis of the stream power law parameters based on worldwide 10Be denudation rates. Geomorphology 268, 184–196. https://doi.org/10.1016/j.geomorph.2016.05.035.

Howard, A.D., 1994. A detachment-limited model of drainage basin evolution. Water Resour. Res. 30, 2261–2285. https://doi.org/10.1029/94WR00757.

Howard, A.D., Kerby, G., 1983. Channel changes in badlands. GSA Bull. 94, 739–752. https://doi.org/10.1130/0016-7606(1983)94<739:CCIB>2.0.CO;2.

Kirby, E., Whipple, K.X., 2012. Expression of active tectonics in erosional landscapes. J. Struct. Geol. 44, 54–75. https://doi.org/10.1016/j.jsg.2012.07.009.

Lague, D., 2014. The stream power river incision model: evidence, theory and beyond. Earth Surf. Process. Landf. 39, 38–61. https://doi.org/10.1002/esp.3462.

Lague, D., Hovius, N., Davy, P., 2005. Discharge, discharge variability, and the bedrock channel profile. J. Geophys. Res. Earth Surf. 110. https://doi.org/10.1029/2004JF000259.

Larimer, J.E., Yanites, B.J., Phillips, W., Mittelstaedt, E., 2019. Late Miocene rejuvenation of central Idaho landscape evolution: A case for surface processes driven by plume-lithosphere interaction. Lithosphere 11, 59–72. https://doi.org/10.1130/L746.1.

Lavé, J., Avouac, J.P., 2001. Fluvial incision and tectonic uplift across the Himalayas of central Nepal. J. Geophys. Res. Solid Earth 106, 26561–26591. https://doi.org/10.1029/2001JB000359.

Mitchell, N.A., Yanites, B.J., 2019. Spatially Variable Increase in Rock Uplift in the Northern U.S. Cordillera Recorded in the Distribution of River Knickpoints and Incision Depths. J. Geophys. Res. Earth Surf. 124, 1238–1260. https://doi.org/10.1029/2018JF004880.

Montgomery, D.R., Foufoula-Georgiou, E., 1993. Channel network source representation using digital elevation models. Water Resour. Res. 29, 3925–3934. https://doi.org/10.1029/93WR02463.

Niemann, J.D., Gasparini, N.M., Tucker, G.E., Bras, R.L., 2001. A quantitative evaluation of Playfair's law and its use in testing long-term stream erosion models. Earth Surf. Process. Landf. 26, 1317–1332. https://doi.org/10.1002/esp.272.

Ouimet, W.B., Whipple, K.X., Granger, D.E., 2009. Beyond threshold hillslopes: Channel adjustment to base-level fall in tectonically active mountain ranges. Geology 37, 579–582. https://doi.org/10.1130/G30013A.1.

Perne, M., Covington, M.D., Thaler, E.A., Myre, J.M., 2017. Steady state, erosional continuity, and the topography of landscapes developed in layered rocks. Earth Surf. Dyn. 5, 85–100. https://doi.org/10.5194/esurf-5-85-2017.

Perron, J.T., Royden, L., 2013. An integral approach to bedrock river profile analysis. Earth Surf. Process. Landf. 38, 570–576. https://doi.org/10.1002/esp.3302.

Rossi, M.W., Quigley, M.C., Fletcher, J.M., Whipple, K.X., Díaz-Torres, J.J., Seiler, C., Fifield, L.K., Heimsath, A.M., 2017. Along-strike variation in catchment morphology and cosmogenic denudation rates reveal the pattern and history of footwall uplift, Main Gulf Escarpment, Baja California. Geol. Soc. Am. Bull. 129, 837–854. https://doi.org/10.1130/B31373.1.

Rossi, M.W., Whipple, K.X., Vivoni, E.R., 2016. Precipitation and evapotranspiration controls on daily runoff variability in the contiguous United States and Puerto Rico. J. Geophys. Res. Earth Surf. 121, 128–145. https://doi.org/10.1002/2015JF003446.

Roy, S.G., Tucker, G.E., Koons, P.O., Smith, S.M., Upton, P., 2016. A fault runs through it: Modeling the influence of rock strength and grain-size distribution in a fault-damaged landscape. J. Geophys. Res. Earth Surf. 121, 1911–1930. https://doi.org/10.1002/2015JF003662.

Royden, L., Taylor Perron, J., 2013. Solutions of the stream power equation and application to the evolution of river longitudinal profiles. J. Geophys. Res. Earth Surf. 118, 497–518. https://doi.org/10.1002/jgrf.20031.

Schoenbohm, L.M., Whipple, K.X., Burchfiel, B.C., Chen, L., 2004. Geomorphic constraints on surface uplift, exhumation, and plateau growth in the Red River region, Yunnan Province, China. Geol. Soc. Am. Bull. 116, 895. https://doi.org/10.1130/B25364.1.

Sklar, L.S., Dietrich, W.E., 2001. Sediment and rock strength controls on river incision into bedrock. Geology 29: 1087-1090.

Snyder, N.P., 2000. Landscape response to tectonic forcing: Digital elevation model analysis of stream profiles in the Mendocino triple junction region, northern California. Geol. Soc. Am. Bull. 14.

Stock, J.D., Montgomery, D.R., 1999. Geologic constraints on bedrock river incision using the stream power law. J. Geophys. Res. Solid Earth 104, 4983–4993. https://doi.org/10.1029/98JB02139.

Whipple, K.X., Forte, A.M., DiBiase, R.A., Gasparini, N.M., Ouimet, W.B., 2017. Timescales of landscape response to divide migration and drainage capture: Implications for the role of divide mobility in landscape evolution: Landscape Response to Divide Mobility. J. Geophys. Res. Earth Surf. 122, 248–273. https://doi.org/10.1002/2016JF003973.

Whipple, K.X., Tucker, G.E., 1999. Dynamics of the stream-power river incision model: Implications for height limits of mountain ranges, landscape response timescales, and research needs. J. Geophys. Res. Solid Earth 104, 17661–17674. https://doi.org/10.1029/1999JB900120.

Whittaker, A.C., 2012. How do landscapes record tectonics and climate? Lithosphere 4, 160–164. https://doi.org/10.1130/RF.L003.1.

Willett, S.D., McCoy, S.W., Perron, J.T., Goren, L., Chen, C.-Y., 2014. Dynamic Reorganization of River Basins. Science 343, 1248765–1248765. https://doi.org/10.1126/science.1248765.

Wobus, C., Whipple, K.X., Kirby, E., Snyder, N., Johnson, J., Spyropolou, K., Crosby, B., Sheehan, D., 2006. Tectonics from topography: Procedures, promise, and pitfalls, in: Tectonics, Climate, and Landscape Evolution. Geological Society of America. https://doi.org/10.1130/2006.2398(04).

Yang, R., Willett, S.D., Goren, L., 2015. In situ low-relief landscape formation as a result of river network disruption. Nature 520, 526–529. https://doi.org/10.1038/nature14354.

Yanites, B.J., Becker, J.K., Madritsch, H., Schnellmann, M., Ehlers, T.A., 2017. Lithologic Effects on Landscape Response to Base Level Changes: A Modeling Study in the Context of the Eastern Jura Mountains, Switzerland: Lithologic effect on landscape evolution. J. Geophys. Res. Earth Surf. 122, 2196–2222. https://doi.org/10.1002/2016JF004101.

Vita

A native of New Jersey, Josh Wolpert received a Bachelor of Arts degree in geosciences from Hamilton College in 2016. After working for two years, he pursued graduate studies at Louisiana State University in the fall of 2018 under Dr. Adam Forte. Josh anticipates graduating from LSU in August 2020 and plans to pursue a Ph.D.